

DLG1 functions upstream of SDCCAG3 and IFT20 to control targeting of polycystin-2 to the primary cilium

Csenge K. Rezi¹, Mariam G. Aslanyan², Gaurav D. Diwan^{3,4}, Tao Cheng⁵, Mohamed Chamli¹, Kathrin Junger⁶, Zeinab Anvarian¹, Esben Lorentzen⁷, Kleo B. Pauly¹, Yasmin Afshar-Bahadori¹, Eduardo F. A. Fernandes⁸, Feng Qian⁹, Sébastien Tosi¹⁰, Søren T. Christensen¹, Stine F. Pedersen¹, Kristian Strømgaard⁸, Robert B. Russell^{3,4}, Jeffrey H. Miner⁵, Moe R. Mahjoub⁵, Karsten Boldt⁶, Ronald Roepman², Lotte B. Pedersen^{1,*}

¹Department of Biology, University of Copenhagen, Denmark

²Department of Human Genetics, Radboud Institute for Molecular Life Sciences, Radboud University Medical Center, Nijmegen, Netherlands

³BioQuant and ⁴Biochemistry Center (BZH), Heidelberg University, Heidelberg, Germany

⁵Department of Medicine (Nephrology Division) and Department of Cell Biology and Physiology, Washington University, St Louis, MO, USA

⁶Institute for Ophthalmic Research, Eberhard Karl University of Tübingen, Tübingen, Germany

⁷Department of Molecular Biology and Genetics - Protein Science, Aarhus University, Denmark

⁸Center for Biopharmaceuticals, Department of Drug Design and Pharmacology, University of Copenhagen, Denmark

⁹Division of Nephrology, Department of Medicine, University of Maryland School of Medicine, Baltimore, MD, USA

¹⁰Danish BioImaging Infrastructure Image Analysis Core Facility (DBI-INFRA IACF), University of Copenhagen, Denmark

***Lead contact:** lbpedersen@bio.ku.dk

Keywords: DLG1, primary cilia, SDCCAG3, IFT20, retromer, polycystin-2, kidney epithelium, CAKUT

Summary

Polarized vesicular trafficking directs specific receptors and ion channels to the primary cilium, but the underlying mechanisms are poorly understood. Here we identify a key role for discs large MAGUK scaffold protein 1 (DLG1), a core component of the Scribble polarity complex, in regulating ciliary protein trafficking in kidney epithelial cells. Conditional knockout of *Dlg1* in mouse kidney caused ciliary elongation and cystogenesis, and cell-based proximity labelling proteomics and fluorescence microscopy showed alterations in the ciliary proteome upon loss of DLG1. Specifically, serologically defined colon cancer antigen-3 (SDCCAG3) and intraflagellar transport protein 20 (IFT20), previously implicated in ciliary targeting of polycystin-2 (PC2), as well as PC2 itself, were reduced in cilia of DLG1 deficient cells compared to control cells. This phenotype was recapitulated *in vivo* and rescuable by re-expression of wildtype DLG1, but not a Congenital Anomalies of the Kidney and Urinary Tract (CAKUT)-associated DLG1 missense variant. Moreover, using biochemical approaches and Alpha Fold modelling we provide evidence that DLG1 associates physically with SDCCAG3 and IFT20, which in turn bind directly to each other. Our work thus identifies a key role for DLG1 in mediating ciliary targeting of PC2 and other proteins and implicates ciliary dysfunction as a possible contributing factor to CAKUT.

Introduction

Primary cilia are microtubule-based sensory organelles that protrude from the surface of many different vertebrate cell types, including kidney epithelial cells, and play essential roles in regulating various signalling pathways during embryonic development and adult homeostasis. Mutations in ciliary genes lead to deregulated signaling, in turn causing diseases known as ciliopathies. While dysfunctional cilia affect most organs in the body, renal involvement is a key feature of many ciliopathies ¹. For example, autosomal dominant polycystic kidney disease (AD-PKD), one of the most common human monogenic diseases affecting ca. 1:1000 live births, is caused by mutations in *PKD1* or *PKD2* encoding the cilium-localized transmembrane proteins polycystin-1 (PC1) and polycystin-2 (PC2), respectively, which form a heterodimeric calcium-permeable nonselective cation channel complex essential for tubular differentiation, polarity and diameter in the kidney ²⁻⁵.

Cilia are compartmentalized organelles that are thought to be devoid of protein synthesis machinery, and appropriate trafficking of PC1 and PC2, as well as other ciliary signaling receptors, ion channels and transporters, from their site of synthesis in the ER/Golgi to the ciliary compartment is essential for ciliary biogenesis and function. For example, a mutation that specifically impairs ciliary localization of PC2, one of the best studied ciliary ion channels, causes PKD in mice ⁶. Additional studies have addressed the molecular mechanisms by which PC2 and other ciliary transmembrane proteins, such as G-protein coupled receptors (GPCRs), are sorted and transported from their site of synthesis in the ER/Golgi to the cilium. These studies have revealed a remarkable complexity and diversity in the mechanisms by which different transmembrane proteins are targeted and transported to the primary cilium ⁷⁻⁹. In the case of PC2, studies of its glycosylation pattern indicated that PC2-containing vesicles destined to the cilium are initially released from the cis-Golgi compartment instead of the trans-Golgi network (TGN) ^{10,11} although this was questioned by

others¹². Regardless, it is believed that shortly after synthesis, PC2 interacts with the ciliary IFT-B subunit IFT20, which is anchored to the cis-Golgi compartment by golgin protein GMAP210/TRIP11, and facilitates the transport of PC2 to the base of the primary cilium^{13,14}. Following sorting at the cis-Golgi or TGN, PC2-containing vesicles are thought to be directed towards the plasma membrane or recycling endosomes before PC2 is delivered at the ciliary base where it docks at the transition fibers before being imported into the cilium^{6,7,9}. Consistent with recycling endosomes playing a critical role in conferring PC2 targeting to the primary cilium, disruption of recycling endosome-associated proteins, such as components of the retromer and biogenesis of lysosome-related organelles complex 1 (BLOC-1) complexes, or the Rab family small GTPases RAB8 and RAB11, reduces ciliary PC2 levels^{7,11,15,16}. Whether and how components located at the plasma membrane contribute to ciliary PC2 trafficking is largely unknown.

Discs large MAGUK scaffold protein 1 (DLG1) is a scaffold protein that belongs to the membrane-associated guanylate kinase homolog (MAGUK) family and is composed of a LIN-2,-7 (L27) domain, three postsynaptic density-95/discs large/zona occludens-1 (PDZ) domains, a SRC homology 3 (SH3) domain and a catalytically inactive guanylate kinase (GUK) domain. First described in *Drosophila*, this evolutionarily conserved scaffold protein is well known for its role in apical-basal polarity establishment and maintenance in epithelial cells, where it forms a complex with SCRIB and LGL at the basolateral membrane below the adherens junctions¹⁷. Consistent with its domain structure, the DLG1 interaction network is vast, and its function extends beyond epithelial cell polarity establishment. For example, in neurons DLG1 localizes to both the presynaptic and postsynaptic membranes and controls localization and clustering of glutamate receptors and potassium channels by mediating interaction between receptors and intracellular proteins¹⁸⁻²². Several studies also suggested that DLG1 localizes to the cilium-centrosome axis. For example, in HT1299 cells DLG1 was

reported to localize to the mitotic centrosome in a PTEN-NEK6-Eg5 dependent manner²³, whereas three independent studies found DLG1 in the ciliary proteome of cultured mouse kidney inner medullary collecting duct 3 (IMCD3) cells^{24,25} and photoreceptor outer segments²⁶, which are modified primary cilia. DLG1 also binds directly to kinesin-3 motor KIF13B²⁷, which was shown previously to localize dynamically to the primary cilium where it regulated ciliary composition and signalling^{28,29}. However, cilium-associated functions for DLG1 have so far not been reported.

The physiological importance of DLG1 in vertebrates is highlighted by the fact that *Dlg1* loss in the mouse causes complete neonatal lethality due to severe defects in e.g. craniofacial development and formation of urogenital organs³⁰⁻³². In humans, *DLG1* was identified as a susceptibility gene for congenital anomalies of the kidney and urinary tract (CAKUT)³³, and a missense variant in DLG1 (p.T489R) was indeed identified in patients with CAKUT³⁴. Furthermore, *DLG1* is deleted in the 3q29 microdeletion syndrome that is characterized by mild-to-moderate mental retardation, a long and narrow face, as well as additional phenotypes such as microcephaly, cleft lip and palate, horseshoe kidney and hypospadias³⁵. However, it is unclear whether some of these phenotypes are linked to ciliary defects.

Here we investigated a potential role for DLG1 in ciliary biogenesis and function by using a kidney specific conditional *Dlg1* mouse knockout model, as well as cultured kidney epithelial cells. Loss of *Dlg1* in mouse kidney caused ciliary elongation and cystogenesis, and cell-based proximity labelling proteomics and fluorescence microscopy showed alterations in the ciliary proteome upon loss of DLG1. Specifically, SDCCAG3, IFT20 and PC2 were reduced in cilia of DLG1 deficient cells - a phenotype that was recapitulated *in vivo* and rescuable by re-expression of wildtype DLG1, but not a CAKUT-associated DLG1 missense variant. Despite its role in regulating ciliary length and composition in kidney epithelial cells,

DLG1 was primarily localized to the lateral plasma membrane in these cells. Finally, in agreement with its role in promoting ciliary localization of SDCCAG3 and IFT20, biochemical approaches and Alpha Fold modelling indicated that DLG1 associates physically with SDCCAG3 and IFT20, which in turn bind directly to each other. Our work thus identifies a key role for DLG1, located at the lateral plasma membrane, in mediating ciliary targeting of PC2 and other proteins and implicates ciliary dysfunction as a possible contributing factor to CAKUT.

Results

Kidney-specific ablation of *Dlg1* in mouse causes ciliary elongation. To investigate possible ciliary functions for DLG1, we analyzed kidneys from *Pax3Cre-Dlg1^{F/F}* mice in which *Dlg1* is conditionally knocked out in the majority of kidney cells, including all nephron (but not ureteric bud) epithelial cell derivatives. These mice display a congenital hydronephrosis phenotype (Figure 1A) similar to that observed in the global *Dlg1^{-/-}* mutant mice³¹, as well as tubular dilations that appeared to be pre-cystic³⁶. The *Pax3Cre* transgene is also active in urogenital mesenchyme, and it was concluded that the lack of DLG1 in these cells results in the observed structural and functional defects in the ureter that cause hydronephrosis³⁶. Loss of DLG1 resulted in a significant increase in cilia length in nephron epithelia (Figure 1B, C), indicating that DLG1 plays an essential role in regulating ciliary biogenesis and/or maintenance during kidney development *in vivo*. Supportively, knock out of *Dlg1* in mouse kidney cortical collecting duct (mCCD) cells³⁷ did not affect ciliation frequency but led to significant ciliary lengthening when cells were grown on transwell filters, which ensures full cell polarization, a phenotype that was rescued by stable re-expression of mCherry-DLG1 (Figure 1D-G). In contrast, under standard culture conditions the *Dlg1^{-/-}* mCCD cells displayed cilia of normal length (Figure S1A), indicating that the ciliary length phenotype manifests itself only when cells are fully polarized. Quantitative RT-PCR analysis showed that in addition to *Dlg1*, mCCD cells also express *Dlg4* and a small amount *Dlg3*, but the relative expression levels of these mRNAs and of *Dlg2* were not altered in the *Dlg1^{-/-}* cells relative to wild type (WT) cells (Figure S1B, C). Thus, the ciliary length phenotype observed in the *Dlg1^{-/-}* cells is not caused by altered expression of *Dlg2*, 3 or 4.

DLG1 localizes to the lateral plasma membrane in polarized kidney epithelial cells. To address how DLG1 might regulate ciliary length we investigated its subcellular localization in transwell filter-grown mCCD cells by immunofluorescence microscopy (IFM) analysis.

Under these conditions endogenous DLG1 localized to the lateral membrane as expected and was not detected at the cilium-centrosome axis (Figure S1C). In contrast, eGFP-DLG1 transiently overexpressed in retinal pigment epithelial (RPE1) cells was highly concentrated at the base of and within the cilium (Figure S1E), indicating that DLG localizes to the cilium-centrosome axis under some conditions, in agreement with previous reports²⁴⁻²⁶. Taken together our results suggest that DLG1 regulates ciliary length in polarized kidney epithelial cells indirectly, i.e. at the level of the lateral plasma membrane.

Loss of DLG1 causes altered ciliary protein content in IMCD3 cells. Ciliary length control is complex and regulated by a variety of factors and signaling pathways that modulate the polymerization/depolymerization of the ciliary axoneme or affect ciliary membrane dynamics; changes in ciliary protein composition that affect signalling output can therefore also affect ciliary length^{38,39}. To investigate how DLG1 might affect ciliary protein composition, we used an unbiased cilium-targeted proximity labelling approach²⁴ by taking advantage of previously described IMCD3 cell lines stably expressing a ciliary NPHP3[residues 1-203]-BioID2 fusion protein (hereafter called cilia-BioID2) or BioID2 alone (hereafter called BioID2)⁴⁰. We then knocked out *Dlg1* in these lines with the aim of determining how loss of DLG1 affects the ciliary proteome. Western blot analysis confirmed the loss of DLG1 in both the cilia-BioID2 and BioID2 *Dlg1*^{-/-} lines (Figure S2A). Meanwhile, IFM analysis of serum-starved cells incubated with biotin and stained with an antibody against ARL13B (ciliary membrane marker), and green-fluorescent streptavidin showed prominent ciliary enrichment of biotinylated proteins in both cilia-BioID2 lines, whereas biotinylated proteins were confined to the cell body of the BioID2 lines, as expected (Figure S2B). Under these conditions we did not observe any differences between WT and *Dlg1*^{-/-} lines with respect to ciliary length (Figure S2C) and ciliation frequency (Figure S2D), as observed in standard cultures of mCCD cells (Figure S1A). Finally, by quantitative RT-PCR

we found that IMCD3 cells express similar amounts of *Dlg1* and *Dlg4* (Figure S2E, F) and knockout of *Dlg1* did not cause altered expression of *Dlg2*, *3* or *4* in these cells (Figure S2G, H).

Having validated our WT and *Dlg1*^{-/-} cilia-BioID2 and BioID2 lines, we next analyzed the ciliary proteome of these cells by subjecting them to biotin labeling followed by streptavidin pull-down and mass spectrometry. Mass spectrometry analysis resulted in the identification of a total of 2100 proteins across 6 experimental replicates per cell line. Our analysis focused solely on proteins that are potentially altered in the primary cilium; therefore, we disregarded the proteins that were significantly altered in the BioID2 control condition. These were further subdivided into three Tiers based on stringency criteria. Tier 1 (q-value ≤ 0.05 and Sign. A ≤ 0.05) comprised 118 highly significantly altered proteins, from which 84 proteins were depleted from the cilium, whereas 34 proteins were enriched (Figure 2A). The rest of the proteins were divided into Tier 2 (Sign. A ≤ 0.05), Tier 3 (q-value ≤ 0.05), and non-significant (NS) when a less stringent cut-off was applied (Figure 2A, Supplementary Table S1). Using the Tier 1 proteins identified in our dataset, a comprehensive GO term enrichment analysis was performed to pinpoint the functional roles of the proteins regarding DLG1's impact on cilium composition. This analysis focused on the two GO categories: Biological Process (BP) and Cellular Component (CC) (Figure 2B, C). The BP terms were, in turn, analyzed separately for the depleted and enriched proteins within the cilium (Figure 2B). For the depleted proteins, the significant BP terms were pertaining to intraciliary transport, cilia assembly and organization as well several signaling pathways. Moreover, in the GO-CC term category, 15 terms were significant, out of which seven terms were associated with ciliary components (Figure 2C). On the other hand, for the enriched proteins, BP terms related to the regulation of cell cycle transitions and mitochondrial gene expression were highly significant (Figure 2B). Altogether, the proximity labeling approach

yielded a dataset indicating a role for DLG1 in regulating ciliary composition in IMCD3 cells.

DLG1 is required for ciliary targeting of SDCCAG3 and IFT20 in kidney epithelial cells. To validate the results of our proximity labelling proteomics analysis, we initially focused on the Tier 1 candidates SDCCAG3 and IFT20, which both appeared to be significantly depleted from cilia of *Dlg1*^{-/-} cells compared to WT (Figure 2A; Supplementary Table S1). SDCCAG3 is a known component of the retromer complex that binds the core retromer subunit VPS35⁴¹, and was shown to localize to primary cilia in cultured mammalian cells, including IMCD3 cells, where it also promoted ciliary targeting of PC2¹⁵. Similarly, IFT20 has a well-established role in conferring targeting of PC2 from the Golgi to the primary cilium^{7,13,14} and is also part of the IFT-B complex involved in IFT within cilia⁴². Analysis of ciliated *Dlg1*^{-/-} and WT cilia-BioID2 IMCD3 cells by IFM with antibodies specific for SDCCAG3 confirmed that its ciliary localization is significantly reduced in the *Dlg1*^{-/-} cells compared to WT (Figure 3A, B), whereas total cellular levels were unchanged (Figure 3C). Stable expression of mCherry-DLG1 in the *Dlg1*^{-/-} cilia-BioID2 IMCD3 cells could restore ciliary levels of SDCCAG3 to normal (Figure 3A, B, D), and similar results were obtained in mCCD cells although SDCCAG3 seemed to be localizing preferentially to the ciliary base in these cells (Figure 3E-G). Using similar approaches, we confirmed that loss of DLG1 causes reduced ciliary base levels of IFT20 in mCCD cells but not cilia-BioID2 IMCD3 cells (Figure S3A-D). The reason for this cell-type specificity is unclear, but we note that our cilia-BioID2 proximity labelling proteomics analysis indicated a rather modest decrease in ciliary IFT20 levels in *Dlg1*^{-/-} cilia-BioID2 IMCD3 cells compared to WT (Figure 2A; Supplementary Table S1), consistent with a relatively mild impact of DLG1 loss on ciliary IFT20 localization in these cells. On the other hand, IFM analysis of kidney sections from WT and *Pax3Cre-Dlg1*^{F/F} mice showed that ciliary levels of SDCCAG3 and IFT20 are

significantly reduced in the *Dlg1* knockout compared to control (Figure 4), indicating that DLG1 promotes ciliary targeting of SDCCAG3 as well as IFT20 *in vivo*. Since DLG1 was previously shown to interact physically and functionally with exocyst complex component SEC8^{43,44}, which in turn mediates ciliary membrane biogenesis and PC2 trafficking^{7,45,46}, we also analyzed whether loss of DLG1 affected ciliary presence of SEC8 in cilia-BioID2 IMCD3 or mCCD cells. However, while this analysis confirmed that SEC8 is concentrated at the ciliary base, we did not observe any significant change in ciliary base levels of SEC8 in *Dlg1*^{-/-} cells compared to WT cells (Figure S4). We conclude that DLG1 is required for localizing SDCCAG3 and IFT20, but not SEC8, to the primary cilium of kidney epithelial cells *in vitro* and *in vivo*.

Loss of or acute inhibition of DLG1 impairs ciliary targeting of PC2. Given the known roles of SDCCAG3 and IFT20 in promoting vesicular trafficking of PC2 to the primary cilium¹³⁻¹⁵, we asked if DLG1 regulates ciliary PC2 trafficking. Although PC2 was not detected in our cilia-BioID2 proximity labelling dataset from IMCD3 cells (Figure 2A; Supplementary Table S1), we reasoned this could be due to technical reasons or the cell line used. We therefore used mCCD cells to directly test if inhibition or depletion of DLG1 affected ciliary PC2 levels. First, we cultivated our WT, *Dlg1*^{-/-} and rescue mCCD lines on transwell filters to ensure full polarization of the cells. Confocal 3D imaging showed that the cells were indeed fully polarized under these conditions, and no apparent polarity defects were observed in the *Dlg1*^{-/-} cells compared to the WT and rescue line (Figure 5A, B). Moreover, the transwell filter-grown *Dlg1*^{-/-} cells also displayed significantly reduced ciliary levels of PC2 compared to the WT cells and this phenotype was rescued by stable expression of mCherry-DLG1 (Figure 5C, D). For robust and unbiased quantification of ciliary PC2 levels, we employed a MATLAB-based approach (see Material and Methods for details) for automatic and high throughput quantitative analysis of ciliary fluorescent staining intensity in

transwell filter-grown mCCD cells. Using this approach, we were also able to confirm our results obtained for SDCCAG3 in mCCD cells grown under standard culture conditions, namely a significantly reduced ciliary presence of SDCCAG3 in *Dlg1*^{-/-} cells compared to WT and rescue lines (Figure 5E, F).

To confirm that DLG1 regulates ciliary PC2 trafficking, we took advantage of two previously described peptide inhibitors, AVLX-144 (ReTat-N-Dimer) and Tat-N-dimer⁴⁷ to specifically block the first and second PDZ domain of DLG1 in ciliated WT mCCD cells. We subsequently analyzed the cells by IFM and staining for PC2 in the treated cells; the cilium was visualized by staining with acetylated α -tubulin antibody. We found that treatment of mCCD ciliated cells with both AVLX-144 and Tat-N-Dimer caused a significant depletion of PC2 from the ciliary base and along the cilium. Importantly, incubation with the control peptide AVLX-144-AA, which is a structurally similar to AVLX-144, but non-binding to PDZ domains⁴⁸, did not affect PC2 ciliary levels (Figure S5). This result indicates that DLG1 is indeed required for targeting of PC2 to the primary cilium, and that the impaired ciliary targeting of PC2 to the cilium observed upon DLG1 inhibition is not secondary to cytokinesis^{49,50} or polarity defects¹⁸.

We conclude that DLG1 is required for targeting PC2 to the primary cilium of kidney epithelial cells, and that the alterations in ciliary composition observed in *Dlg1*^{-/-} cells are not due to cytokinesis or polarity defects. Furthermore, we conclude that DLG1-mediate ciliary targeting of PC2 requires DLG1's first two PDZ domains.

A CAKUT-associated DLG1^{T507R/T489R} missense variant fails to rescue the ciliary phenotype of *Dlg1*^{-/-} cells. A previous study identified a DLG1 missense mutation (p.T489R; hereafter referred to as DLG1^{T489R}) in patients with CAKUT³⁴. To investigate a possible ciliary involvement in this disorder, we tested if exogenous expression of the rat equivalent of

this missense variant, DLG1^{T507R} (Figure 6A), could rescue the ciliary phenotype of *Dlg1*^{-/-} cells. To this end, we generated a lentiviral construct that we used for stable expression of mCherry-DLG1^{T507R} in the *Dlg1*^{-/-} mCCD cells (Figure 6B). Interestingly, while stable expression of mCherry-tagged WT DLG1 fully restored ciliary base levels of IFT20 (Figure S3C, D) and SDCCAG3 (Figure 3E, F) in mCCD cells, this was not the case for the DLG1^{T507R} variant (Figure 6C-F). This suggests that ciliary defects may contribute to the CAKUT disease aetiology of patients harbouring the DLG1^{T489R} mutation and demonstrates a possible ciliary involvement in CAKUT.

Loss of DLG1 leads to constitutive phosphorylation of MAP3K7. Upon analysing the GO-BP terms of our proteomics data (Figure 2B) we noticed that several proteins responsible for regulating MAP kinase activity, such as mitogen-activated protein kinase kinase kinase 7 (MAP3K7, also known as Transforming growth factor beta (TGFβ) Activated Kinase 1, TAK1), are diminished in the primary cilium of *Dlg1*^{-/-} cells. As MAP3K7 is linked to the pathogenesis of kidney fibrosis stimulated by TGFβ ligands^{51,52} and since TGFβ signalling is orchestrated by the primary cilium^{53,54} we investigated the potential impact of *Dlg1* loss on TGFβ signalling. Upon stimulation with TGFβ-1 ligand, we observed that activation of SMAD2 as evaluated by its phosphorylation on Ser465/467 in the canonical branch of TGFβ signalling was largely unaffected in ciliated *Dlg1*^{-/-} as compared to WT mCCD cells (Figure 6G, H). In contrast, we observed that phosphorylation of MAP3K7 on Thr184/187 and S412 marking full activation of this MAP kinase was significantly increased in unstimulated *Dlg1*^{-/-} cells as compared to WT cells (Figure 6I-J). These results indicate that DLG1 takes part in the regulation of sub-pathways in TGFβ signalling, although further studies are needed to delineate the mechanisms by which DLG1 restricts basal levels of MAP3K7 activation, and whether such mechanisms are controlled at the level of primary cilia.

DLG1 associates physically with SDCCAG3 and IFT20. Finally, to address the mechanism by which DLG1 promotes targeting of SDCCAG3 and IFT20 to the primary cilium, we tested if DLG1 interacts physically with these proteins. Indeed, immunoprecipitation (IP) of lysates from HEK293T cells co-expressing GFP-DLG1 and SDCCAG3 or IFT20 fusion proteins indicated that DLG1 interacts physically with both SDCCAG3 and IFT20 (Figure 7A, B). Similarly, IP analysis in HEK293T cells demonstrated physical interaction between SDCCAG3 and IFT20 (Figure 7A). To determine the molecular basis for these interactions we used Alpha Fold modelling⁵⁵ and identified a high confidence interaction between SDCCAG3 and IFT20 (Figure 7C; Figure S6) but did not obtain strong evidence indicative of direct binding of these two proteins to DLG1. Moreover, the predicted interaction between IFT20 and SDCCAG3 is mutually exclusive with binding of IFT20 to its known partner within the IFT-B complex, IFT54⁵⁶ (Figure 7C). IFT20 was shown previously to interact physically with the BLOC-1 complex⁷, and the BLOC-1 complex subunit DTNBP1 (dysbindin) binds directly to DTNA and DTNB (α - and β -dystrobrevin, respectively) of the dystrophin-glycoprotein complex (DGC)⁵⁷. Interestingly, we and others have previously shown that DLG1 as well as its direct interactor, KIF13B, bind physically to components of the DGC, including UTRN, DTNA and DTNB^{58,59}. Furthermore, a high throughput study indicated that SDCCAG3 also binds DTNBP1⁶⁰. Therefore, we hypothesize that DLG1 may associate physically with IFT20 and SDCCAG3 through DTNBP1-DTNA/B interactions but more work is needed to clarify this. In summary, DLG1 associates, at least indirectly, with SDCCAG3 and IFT20, which in turn bind directly to each other. In summary, SDCCAG3 and IFT20 form a hetero-dimeric complex that associates, at least indirectly, with DLG1.

Discussion

Here we demonstrated that DLG1 is important for regulating the length and composition of primary cilia in kidney epithelial cells, both in cultured cells and *in vivo*. Using an unbiased cilium-targeted proteomics approach, we show that loss of DLG1 in IMCD3 cells causes altered ciliary protein content with most of the affected proteins being diminished in the cilium of *Dlg1*^{-/-} cells. Specifically, loss DLG1 lead to reduced ciliary levels of SDCCAG3 and IFT20, which have both been shown to confer ciliary targeting of PC2¹³⁻¹⁵. Consistently, we also established a requirement for DLG1 in promoting ciliary targeting of PC2 in mCCD cells. Reduced ciliary presence of polycystins may at least be partly responsible for the observed ciliary length phenotype of DLG1-deficient cells⁶¹ although alternative mechanisms cannot be excluded. From a human disease perspective PC2 is highly relevant as mutations in its corresponding gene (*PKD2*) cause AD-PKD⁶², and appropriate ciliary localization of PC2 is critical for its function⁹. SDCCAG3 and IFT20 seem to promote ciliary trafficking of PC2 primarily at the level of the recycling endosome and cis-Golgi^{7,13-15}, and exocyst complex components also impact the ciliary targeting of PC2⁷. The exocyst complex tethers vesicles at target sites before membrane fusion⁶³, and DLG1 binds exocyst complex component SEC8^{43,64}. However, loss of DLG1 did not affect the ciliary base localization of SEC8 in IMCD3 or mCCD cells.

Although DLG1 may localize to primary cilia under some conditions²⁴⁻²⁶, we found that in polarized kidney epithelial cells DLG1 is largely confined to the lateral plasma membrane in agreement with its well-known role as a core component of the Scribble polarity complex. The Scribble complex, which consists of DLG1, Scribble (SCRIB) and lethal giant larvae (LGL), plays a central role in orchestrating epithelial cell polarity⁶⁵, and Scribble complex components were also implicated in protein cargo sorting and vesicle transport. For example, a study in mouse hippocampal neurons found that DLG1 regulates clathrin-mediated endocytosis of AMPA receptors by recruiting myosin VI and AP-2 adaptor

complex to endocytotic vesicles containing these receptors⁶⁶. Furthermore, in *Drosophila* the Scribble complex is required for proper localization of retromer components to endosomes and promotes appropriate sorting of cargo in the retromer pathway⁶⁷, consistent with our finding that DLG1 associates with and regulates ciliary localization of retromer component SDCCAG3. Studies have demonstrated that deficiency of retromer regulator sorting nexin-17 (SNX17) and SDCCAG3 disrupt ciliogenesis^{15,68}. Moreover, the retromer complex interacts with the N-terminal cytoplasmic domain of PC2, and the disruption of this interaction impairs the ciliary localization of PC1¹⁶. Since DLG1 localizes predominantly to the lateral plasma membrane in polarized kidney epithelial cells our results are consistent with a model whereby DLG1 regulates internalization of ciliary cargoes (SDCCAG3, IFT20, PC2) that are transiently transported to this site prior to their onward journey via recycling endosomes to the primary cilium (Figure 7D). Notably, the Na⁺,HCO₃⁻ cotransporter NBCn1 (SLC4A7), which localizes at the lateral membrane and primary cilium of polarized kidney epithelial cells, interacts tightly with DLG1⁶⁹, and multiple retromer components were identified as putative NBCn1 binding partners in GST pulldown assays⁷⁰. Furthermore, our proteomics analysis identified the Na⁺/H⁺ exchanger NHE1(SLC9A1) and the cation channel TRPV4 as Tier 1 candidates depleted from cilia in the *Dlg1*^{-/-} cells (Figure 2; Table S1). This suggests that DLG1 and the retromer complex may regulate ciliary trafficking of a range of ion channels and transporters, in addition to PC2. Future research should be aimed at addressing this possibility.

Epithelial cells rely on highly organized trafficking machinery to maintain their polarity and carry out their epithelial functions. Such trafficking involves several factors, including sorting signals, cytoskeletal network, vesicle tethering complexes, and Rab and Rho GTPases, that determine the final destination of each protein⁷¹. Importantly, the cellular microtubule cytoskeleton of polarized epithelial cells is organized very differently compared

to mesenchymal cells, with microtubules aligning parallel to the apico-basal axis and extending their plus ends towards the basal surface ⁷² (Figure 7D). Therefore, post-Golgi vesicle trafficking in epithelial cells often occurs via indirect transport routes, such as transcytotic or recycling endosomal routes, to ensure delivery of membrane cargo to the apical surface or ciliary compartment ^{7,9,72}. In addition to the lateral plasma membrane functioning as a docking site for ciliary components, prior to their final transport to the cilium, the apical membrane domain may also function as a transit point for ciliary protein trafficking. For example, nephronophthisis proteins NPHP1, NPHP4, and NPHP8 not only localize to the transition zone, but also accumulate at cell junctions, e.g. in polarized kidney epithelial cells ⁷³, where they interact with Crumbs polarity complex components (PATJ, PALS1, PAR6) ⁷⁴, which are concentrated at the apical-lateral border, just above the tight junctions ⁷⁵. Conversely, accumulating evidence suggests that components of the Crumbs complex localize to cilia and regulate ciliary assembly or function ⁷⁶⁻⁷⁸. Notably, our proteomics analysis identified PATJ (INADL) as a Tier 1 candidate depleted from cilia in the *Dlg1*^{-/-} cells (Figure 2; Table S1) and PC2 was also shown to bind to the Crumbs complex component PALS1 ⁷⁹, suggesting that multiple polarity complexes located along the apical-basal border of epithelial cells may function together to regulate ciliary protein cargo transport. More studies will be needed to explore this in more detail and define the precise mechanisms involved.

Our cilia proteomics analysis identified several proteins that affect energy homeostasis and NFκB and TGFβ signaling, and which were depleted from cilia of *Dlg1*^{-/-} cells. These include MAP3K7 (TAK1), whose kinase activity is critical for regulating a variety of cell functions relevant for kidney development and function ⁸⁰. Interestingly, our cell-based assays showed that disruption of DLG1 leads to over-activation of MAP3K7 in line with a recent study, showing that *Dlg1* deficiency in mouse microglial cells impairs

microglial activation and prevents production of inflammatory cytokines⁸¹. Furthermore, multiple lines of evidence have shown that alterations in ciliary length and inactivation of polycystins can cause profound metabolic rewiring in the kidney, which likely contributes to development of PKD⁸²⁻⁸⁴. Nevertheless, if and how altered ciliary length and composition, as well as dysregulated metabolic, NF κ B and TGF β signaling, contribute to the kidney defects observed in *Dlg1* deficient mice and human CAKUT patients with *DLG1* mutations awaits further investigation. However, we note that a more distantly related DLG1 homolog, DLG5, has been implicated in ciliary biogenesis and function as well as CAKUT^{85,86}, substantiating the involvement of cilia and DLG proteins in this disease.

Materials and methods

Mammalian cell culture. Mouse inner medullary collecting duct 3 (IMCD3) cells stably expressing NPHP3[residues 1-203]-BioID2 (hereafter called cilia-BioID2) and BioID2 alone (hereafter called BioID2) have been described previously⁴⁰. IMCD3 cells were cultured in DMEM/F-12, GlutaMAX Supplement (Gibco, cat. #31331-093) medium supplemented with 10% fetal bovine serum (FBS; Gibco, cat. #10438-026) and 1% Penicillin-Streptomycin (Sigma-Aldrich, cat. #P0781). The immortalized mouse cortical collecting duct (mCCD) parental/WT cell line was generously provided by Dr. Eric Féraille (University of Lausanne, Switzerland) and has been described previously³⁷. The mCCD cells were cultured as described in³⁷, and RPE1 cells stably expressing SMO-tRFP⁸⁷ we cultured and transfected as described in²⁹. Human embryonic kidney (HEK) 293T cells were from ATCC (cat. #CRL-3216) and were cultured in high-glucose DMEM (Gibco, cat. #41966-052) supplemented with 10% FBS and 1% Penicillin-Streptomycin.

All cell lines were grown in a 95% humidified incubator at 37 °C with 5% CO₂. To induce ciliogenesis, IMCD3 cells were grown in plain DMEM/F-12, GlutaMAX Supplement for 24 h, while mCCD cells were grown in starvation medium, where the serum and hormone-deprived DMEM/F12, GlutaMAX Supplement medium was supplemented with 5 µg/ml holo-transferrin (Sigma-Aldrich, cat. # T0665) and 60 nM sodium selenite (Sigma-Aldrich, cat. #S5261) for 24 h.

Transwell culture system. For setting up fully polarized epithelial cells, mCCD cells were grown in full DMEM/F-12, Glutamax Supplement medium as described previously, using Thermo Scientific™ Nunc™ Polycarbonate Membrane Inserts in Multidishes (Thermo Scientific, cat. #140652), which have a pore size of 0.4 µm. This was done for a duration of 10 days before proceeding with further experiments. The medium was replaced every 3 to 4 days. For IFM analysis, the polarized mCCD cells were fixed and membrane inserts were excised and treated as described in the general IFM protocol (see below).

Generation of *Dlg1*^{-/-} cell lines. To knock out *Dlg1* in the kidney epithelial cell lines, we employed CRISPR/Cas9 technology and used four sgRNA sequences from the mouse CRISPR “Brie” Knockout Library⁸⁸. The sequences are provided in Table 1. The sgRNA spacers were cloned into pSpCas9(BB)-2A-Puro (PX459) V2.0 plasmid (Addgene, cat. #62988) as described previously⁸⁹. This involved phosphorylating and annealing the two complementary sgRNA oligos, which were then ligated into the BbsI-digested backbone. Then the selected clones were sequenced to verify the spacer sequence. The parental (WT) cilia-BioID2 and BioID2 IMCD3 lines, and the WT mCCD cells were transfected with the Cas9-gRNA plasmids (pool of all four gRNAs) using reverse transfection with Lipofectamine 3000 Transfection Reagent (Invitrogen, cat. #L3000015) according to the manufacturer's instructions. A day after transfection, cells were treated with 2 µg/ml puromycin (Invitrogen, cat. #A11138-03) for 72 h and then tested for DLG1 protein depletion by western blot

analysis. Subsequently, the cells underwent single cell sorting at the FACS Facility at Biotech Research & Innovation Centre (University of Copenhagen, Copenhagen, DK). The selected clones were validated by western blot analysis and Sanger sequencing to confirm the occurrence of the indel event.

Generation of transgenic cell lines. A plasmid containing the full-length rat DLG1 coding sequence⁹⁰ was used as template for cloning the rat *Dlg1* coding sequence into Gateway entry plasmid pENTR220-mCherry-C1 using standard cloning techniques. This entry plasmid was then recombined with pCDH-EF1a-Gateway-IRES-BLAST destination plasmid through LR reaction using the Gateway LR Clonase II Enzyme mix (Invitrogen, cat. #11791020). The cloning vectors used were generously provided by Dr. Kay Oliver Schink (Oslo University Hospital, Norway), and were described in⁹¹. The lentiviral expression plasmids were later subjected to site-directed mutagenesis, performed by GenScript, to create a double-point mutation on the following sites: c.1520C>G and c.1521T>A; p.T507R. Lentiviral particles were generated by co-transfecting the lentiviral expression plasmids with second-generation lentiviral packaging vectors pMD2.G and pCMVΔ-R8.2 into HEK293T cells (kindly provided by Dr. Carlo Rivolta, Institute of Molecular and Clinical Ophthalmology Basel, Switzerland) using Lipofectamine 3000 Transfection Reagent (Invitrogen, cat. #L3000015) according to the manufacturer's instructions. The harvested culture medium containing lentiviral particles coding for either WT DLG1 or DLG1^{T507R} fusion proteins were used to transduce the kidney epithelial cells. Cells were selected using 5-15 μg/ml Blasticidin S (Gibco, cat. #R21001) and expression was confirmed with western blotting and live cell fluorescence microscopy.

BioID2 proximity labeling. We conducted a proximity labeling experiments, which involved the WT and *Dlg1*^{-/-} cilia-BioID2 lines described above, with the WT and *Dlg1*^{-/-} BioID2 lines as negative controls. The cells were plated in 15 cm dishes and cultured in normal medium

containing DMEM/F-12, GlutaMAX Supplement (Gibco, cat. #31331-093) supplemented as described above. Once the cells had reached 80% confluency, they were stimulated for ciliogenesis for 24 h with the medium described above. Proximity labeling was induced overnight by supplementing the medium with 10 μ M Biotin (Sigma-Aldrich, cat. #B4501). The cells were lysed, and samples were prepared for mass spectroscopy according to a previously published BioID2-based proximity labeling protocol ⁴⁰.

Mass spectroscopy and data analysis. The samples were analyzed and proteins were identified according to the method described in ⁴⁰. For proteomics data analysis, we used a custom in-house R script that replicates the analysis using the Perseus software ⁹². The LFQ intensity values were compared for cilia-BioID2 WT samples versus those for cilia-BioID2 *Dlg1*^{-/-} samples and for BioID2 WT samples versus BioID2 *Dlg1*^{-/-} samples. For samples where LFQ intensity values were zero in less than half of the replicates, while having non-zero LFQ intensity values in the other replicates, imputed values were applied drawn from a normal distribution that had a mean that was 1.8 times below the mean of the non-zero values and a standard deviation that was 0.5 times the mean. Subsequently, Student's t-test was used for statistical comparisons between the LFQ intensity values of samples as well as the significance A test to infer samples with outlier log₂ ratios (high or low). After removing the proteins that were significantly altered in the BioID2 comparison, we devised a three-tier system to classify significant proteins from the cilia-BioID2 comparison. Tier 1 proteins were ones where the corrected p-values (Benjamini-Hochberg correction) from the t-test were < 0.05 as well as significance A test p-values were < 0.05. Tier 2 proteins included proteins that only had significance A test p-values < 0.05 and Tier 3 proteins were the ones that only had corrected p-values from the t-test < 0.05.

GO term enrichment analysis. To conduct the analysis, the topGO package ⁹³ in R was utilized on the Tier 1 proteins, comprising 118 proteins in total. The approach involved using

the GO terms (Biological Process – BP and Cellular Component – CC) linked with all the proteins in the proteomics data analysis and carried out an enrichment analysis for each GO category using Fisher’s exact test. Next, a maximum of the top 30 terms were sorted by the Odds ratio and with Fisher’s test corrected p-value < 0.05 and removed the redundancy in the enriched terms to leave only the terms that were specific and perhaps more informative. This was achieved by removing the other terms that were ancestral in the same GO lineage as the term of interest.

Immunofluorescence microscopy analysis and live cell imaging. IMCD3 and mCCD cells were trypsinized (2x concentration, Sigma Aldrich, cat. #T4174), seeded, and grown on 12-mm diameter glass coverslips. Upon reaching 80% confluence, cells were starved for 24 h to induce robust ciliogenesis using the aforementioned media. The coverslips were fixed in 4% paraformaldehyde (PFA; Sigma, cat. #47608) in PBS for 12 min either at room temperature or at 4 °C, washed with PBS, and incubated in permeabilization buffer (0.2% Triton X-100, 1% BSA in PBS) for 12 min before blocking and antibody incubation. The fixed cells were blocked in 2% (w/v) BSA-based blocking buffer, then incubated with primary antibodies diluted in 2% BSA for 1.5-2 h at room temperature or overnight at 4 °C. After extensive washing with PBS, cells were then incubated with secondary antibodies diluted in 2% BSA in PBS for 1 h at room temperature. Last, nuclei were labeled with DAPI (Sigma-Aldrich, cat. #D9542). Antibodies and dilutions used in this study for IFM are listed in Table 1. For IFT20 staining, we followed an IFM protocol method described in ⁹⁴ where we briefly washed the cells with cytoskeletal buffer, then immediately fixed them with ice-cold MeOH inside a -20 °C freezer. For PC2 and SEC8 staining, we used an IFM protocol method described in ⁹⁵. All coverslips were mounted with 6% propyl gallate (Sigma-Aldrich, cat. #P3130) diluted in UltraPure Glycerol (Invitrogen, cat. #15514-001) and 10xPBS and combined with EpreDia Immu-Mount (EpreDia, cat. #9990402) in a 1:12 ratio.

Images of cells seeded on coverslips were obtained with an Olympus BX63 upright microscope equipped with a DP72 color, 12.8 megapixels, 4140x3096 resolution camera, and Olympus UPlanSApo 60x oil microscope objective. Images of the transwell filter-grown polarized epithelial cells were obtained with an Olympus IX83 inverted microscope, equipped with a Yokogawa CSU-W1 confocal scanner unit, ORCA-Flash4.0 V3 Digital CMOS camera (type number: C13440-20CU), and Olympus UPlanSApo 100x oil microscope objective. To prepare the images for publication, we used cellSens 1.18 software for constrained iterative deconvolution and assembled montages with Fiji and Adobe Photoshop 2023.

Live cell imaging of RPE1 cells stably expressing SMO-tRFP and transiently expressing eGFP-DLG1 was done as described in ²⁹.

Immunofluorescence staining of kidney sections. The mouse kidney specimens assayed for ciliary length, SDCCAG3 and IFT20 localization were obtained from *Pax3Cre-Dlg1^{F/F}* mice and control (wildtype) littermates that were previously described ³⁶. For immunofluorescence staining of paraffin-embedded sections, antigen unmasking was performed by boiling the slides in antigen-retrieval buffer (10 mM Tris Base, 1 mM EDTA, and 0.05% Tween-20, pH 9.0) for 30 min. Samples were permeabilized with 0.05% Triton X-100 in PBS (PBS-T) for 10 min at room temperature, incubated in blocking buffer (3.0% BSA and 0.1% Triton X-100 in PBS) for 1 h, followed by staining with primary antibodies against SDCCAG3, IFT20 or acetylated tubulin overnight at 4°C. After 3 washes with PBS-T, samples were incubated with secondary Alexa Fluor dye-conjugated antibodies for 1 h at room temperature. Nuclei were stained with DAPI, and specimens mounted using Mowiol containing n-propyl gallate (Sigma-Aldrich). Images were captured using a Nikon Eclipse Ti-E inverted confocal microscope equipped with a 60x Plan Fluor oil immersion (1.4 NA) and 100x Plan Fluor oil immersion (1.45 NA) objectives. A series of digital optical sections (z-stacks) were captured

using a Hamamatsu ORCA-Fusion Digital CMOS camera at room temperature, and 3D image reconstructions were produced. Images were processed and analyzed using Elements AR 5.21 (Nikon), Adobe Illustrator and Photoshop software.

Quantitative Real-Time PCR (RT-qPCR). Isolation of total RNA was performed using the NucleoSpin RNA II kit (Macherey-Nagel, cat. # 740955.50) following the manufacturer's instructions. RNA was reverse-transcribed using Superscript III Reverse Transcriptase (Invitrogen, cat. #18080-044) and cDNA amplified by qPCR using SYBR Green (Applied Biosystems, cat. #4309155). The qPCR was conducted in triplicate using the QuantStudio 7 Flex Real-Time PCR system with the following steps: 95 °C for 10 min, 40 cycles of [95 °C for 30 sec, 60 °C for 1 min, 72 °C for 30 sec], 95 °C for 1 min. Primer sequences used in this study for RT-qPCR are listed in Table 1. mRNA levels were determined using the comparative threshold cycle (Ct) method, normalizing to GAPDH and 18S ribosomal RNA. The mRNA levels were expressed relative to that in WT mCCD cells.

Inhibition of DLG1. Acute inhibition of DLG1 was done DLG1 using the peptides AVLX-144 (ReTat-N-dimer), Tat-N-dimer and the non-PDZ-binding control AVLX-144-AA previously described in ^{47,48}. Compounds were purchased from WuXi AppTec (Shanghai, China) as a hydrochloride salt and purity was checked by mass-spectrometry. Prior to the inhibitor experiment, the WT mCCD cells were seeded on glass coverslips and allowed to reach 80% confluence. To promote ciliogenesis, the cells were subjected to a 24 h starvation period using the starvation medium outlined previously. After 12 h of starvation, the medium was changed to the inhibitor-supplemented starvation medium and incubated for an additional 12 h. Subsequently, the cells were examined using IFM analysis.

Immunoprecipitation, SDS-PAGE, and western blot analysis. Immunoprecipitation in mCCD and HEK293T cells was carried out as described previously ⁹⁶. except that the

washing buffer contained 0.1% NP-40 instead of 0.5% NP-40. Input and pellet fractions were analyzed by SDS-PAGE and western blotting as described previously⁹⁶ by using antibodies and dilutions as listed in Table 1.

TGF β stimulation assay. Following cell seeding and 24h incubation with starvation medium, the cells were stimulated with 2 ng/mL recombinant human TGF- β 1 (R&D Systems, cat. # 240-B) diluted in starvation medium for varying durations of 30, 60, 90, and 120 minutes or left untreated (0 minute). The cells were later lysed for subsequent analysis using the aforementioned SDS-PAGE and western blotting. The antibodies and dilutions used for this analysis are listed in Table 1.

Quantitative image and statistical analysis. Using IFM images and Fiji software⁹⁷ we measured cilium length, frequency, and relative mean fluorescence intensity (MFI) of relevant antibody-labeled antigens at the cilium or ciliary base in WT, *Dlg1*^{-/-} and rescue IMCD3 and mCCD lines. Unless otherwise stated, the results were confirmed in at least three independent biological replicates. Statistical analyses were performed using GraphPad Prism 10.0.1. For manual quantification of ciliary staining intensities of fluorescent images, the background-corrected MFI was normalized to relevant control cells. The data was tested for Gaussian normality using either D'Agostino's K-squared test or Shapiro–Wilk test. If the data followed a normal distribution, the two-tailed, unpaired Student's t-test was used when comparing two groups, or one-way ANOVA followed by Tukey's multiple comparison tests was used for comparing more than two groups. If the data did not follow a normal distribution, the nonparametric Mann-Whitney test was used when comparing two groups, or the Kruskal-Wallis test with Dunn's multiple pairwise comparison tests was used for comparing more than two groups. All quantitative data are presented as mean \pm standard deviation unless otherwise specified. Differences were considered significant when the p-

value was <0.05 . Quantitative analysis of western blot data was done as described previously⁹⁶.

Automated image analysis and primary cilia intensity measurements. PC2 (Figure 5c and 5D) and SDCCAG3 (Figures 5E and 5F) intensity levels were measured in spinning disk fluorescence microscopy 3D image stacks of transwells-cultured cells acquired from WT, *Dlg1*^{-/-}, and rescue mCCD cell lines in three independent experiments, with a total of 15-25 images and 431-739 cells/cilia analyzed per condition. To minimize any bias and ensure experimental reproducibility, all intensity measurements were performed by a fully automated MATLAB script reporting the mean fluorescence intensity of the protein of interest inside subregions of the identified primary cilia. The functional steps of the script are reported below. First, 1) Nucleus regions were automatically identified (DAPI channel, Gaussian filtering, background subtraction and global thresholding) and 2) primary cilia were accurately segmented (cilia marker channel, Gaussian filtering, and local thresholding) as the brightest 3D objects overlapping a nucleus region. Next, 3) primary cilium bases were identified as the closest cilium voxel to the center of mass of the corresponding nucleus region (assuming an outward growth of the cilia), and 4) primary cilium base regions were defined as the set of cilium voxels within a maximum (user defined) geodesic distance to the corresponding base. Finally, 5) SDCCAG3 and PC2 channels mean intensities were individually measured and reported inside each primary cilium, primary cilium base region, and primary cilium body (whole cilium excluding the base region) after background intensity correction (3D median filtered image subtraction). Example images are shown in Figure S7. The script was developed for this project by Danish Bioimaging Infrastructure Image Analysis Core Facility (DBI-INFRA IACFF) and is available upon request and will soon be available from <https://github.com/DBI-INFRA>.

AlphaFold modeling of protein complexes. Structures of protein complexes shown in Figures 7C and S6B-D were modeled using a local installation of Alphafold v2.1.0^{55,98} using sequences for *Mus musculus* (Mm) or *Homo sapiens* (Hs) DLG1, SDCCAG3, IFT20, and IFT54. Predicted interacting areas were inspected for a low Predicted Alignment Error (PAE) score as the main indicator for confidence. All figures of protein structures were prepared using PyMOL v. 2.5 (Schrodinger LLC, <https://pymol.org>).

Acknowledgments

We thank Søren L. Johansen and Maria S. Holm for expert technical assistance, and Pernille M. H. Olesen, Julie K. T. Sørensen, Søren Bjerg, and Maaryah Iqbal for contributing to the initial stages of this project, and Rachel Giles for helpful discussions and for contributing results that ended up not being included. We are grateful to the Polycystic Kidney Disease Research Resource Consortium (U54DK126114) for providing the anti-PC2 (rabbit polyclonal) antibody, and to Eric Féraillé, Greg Pazour, Christopher Westlake, Kay Oliver Schink, Carlo Rivolta, and Michael Taschner for other reagents. This work was supported by grants NNF18SA0032928 and NNF22OC0080406 from the Novo Nordisk Foundation (LBP, SFP), grant 2032-00115B and 3103-00177B from the Independent Research Fund Denmark (LBP, STC), grant R01-DK108005 from the National Institute of Diabetes and Digestive and Kidney Diseases (MRM), and the European Union's Horizon 2020 research and innovation program Marie Skłodowska-Curie Innovative Training Networks (ITN) grant 861329 (RR, RBR, KB, STC, LBP).

Reagent type (species) or resource	Designation	Source or reference	Identifiers	Additional information
Kidney tissue (<i>Mus musculus</i>)	<i>Pax3-Cre</i> strain with <i>Dlg1</i> ^{+/+} alleles	³⁶	Wild type	C57BL/6J-CBA/J mixed background
Kidney tissue (<i>Mus musculus</i>)	<i>Pax3-Cre</i> strain with <i>Dlg1</i> ^{F/F} alleles	³⁶	<i>Pax3Cre-Dlg1</i> ^{F/F}	C57BL/6J-CBA/J mixed background
Cell line (<i>Mus musculus</i>)	IMCD3 Flp-In	⁴⁰	Wild type (parental)	
Cell line (<i>Mus musculus</i>)	IMCD3 Flp-In w/ cilia-BioID2	⁴⁰	Wild type	
Cell line (<i>Mus musculus</i>)	IMCD3 Flp-In w/ BioID2	⁴⁰	Wild type	
Cell line (<i>Mus musculus</i>)	mCCD	⁹⁹	Wild type (parental)	c11 parental cells
Cell line (<i>Homo sapiens</i>)	HEK293T	ATCC	Cat. #CRL-3216	
Cell line (<i>Mus musculus</i>)	IMCD3 Flp-In w/ DLG1-BioID2	This study	Pool	Generated by Flp-FRT recombination
Cell line (<i>Mus musculus</i>)	IMCD3 Flp-In w/ cilia-BioID2 <i>Dlg1</i> ^{-/-}	This study	Pool of knockout	Generated by CRISPR/Cas9 methodology
Cell line (<i>Mus musculus</i>)	IMCD3 Flp-In w/ BioID2 <i>Dlg1</i> ^{-/-}	This study	Pool of knockout	Generated by CRISPR/Cas9 methodology
Cell line (<i>Mus musculus</i>)	mCCD <i>Dlg1</i> ^{-/-}	This study	Clone A8	Generated by CRISPR/Cas9 methodology
Cell line (<i>Mus musculus</i>)	IMCD3 Flp-In w/ cilia-BioID2 <i>Dlg1</i> ^{-/-} w/ mCherry-DLG1	This study	Pool/rescue line	Generated by lentiviral transduction
Cell line (<i>Mus musculus</i>)	mCCD <i>Dlg1</i> ^{-/-} w/ mCherry-DLG1	This study	Pool/rescue line	Generated by lentiviral transduction
Cell line (<i>Mus musculus</i>)	mCCD <i>Dlg1</i> ^{-/-} w/ mCherry-DLG1 ^{T507R}	This study	Pool/mutant line	Generated by lentiviral transduction
Cell line (<i>Homo sapiens</i>)	hTERT-RPE1 w/SMO-tRFP	⁸⁷	RPE1 SMO-tRFP	
Strain, strain	DH10B	Lab stock	N/A	

background (<i>Escherichia coli</i>)				
Sequence-based reagent	<i>M. musculus Dlg1</i> exon 5 sgRNA target sequence	Eurofins Genomics	sgRNA 1	5'-TTCTCCACAAGTCACAAATG-3'
Sequence-based reagent	<i>M. musculus Dlg1</i> exon 8 sgRNA target sequence	Eurofins Genomics	sgRNA 2	5'-TTGAGTCATCTCCAATGTGT-3'
Sequence-based reagent	<i>M. musculus Dlg1</i> exon 9 sgRNA target sequence	Eurofins Genomics	sgRNA 3	5'-TGCGATTGTATGTGAAAAAG-3'
Sequence-based reagent	<i>M. musculus Dlg1</i> exon 14 sgRNA target sequence	Eurofins Genomics	sgRNA 4	5'-GGGTCGATATTGCGCAACGA-3'
Sequence-based reagent	<i>M. musculus Gapdh</i> RT-qPCR primer sequence	Eurofins Genomics	N/A	sense 5'-TGTCGTCGTGGATCTGAC-3'; antisense 5'-CCTGCTTCACCACCTTCTTG-3'
Sequence-based reagent	<i>M. musculus 18S rRNA</i> RT-qPCR primer sequence	Eurofins Genomics	N/A	sense 5'-GCAATTATCCCCATGAAACG-3'; antisense 5'-AGGGCCTCACTAAACCATCC-3'
Sequence-based reagent	<i>M. musculus Dlg1</i> RT-qPCR primer sequence	Eurofins Genomics	N/A	sense 5'-CGAAGAACAGTCTGGGCTT-3'; antisense 5'-GGGGATCTGTGTCAGTGTGG-3'
Sequence-based reagent	<i>M. musculus Dlg2</i> RT-qPCR primer sequence	Eurofins Genomics	N/A	sense 5'-TGCCTGGCTGGAGTTTACAG-3'; antisense 5'-TTTTACAATGGGGCCTCCGC-3'
Sequence-based reagent	<i>M. musculus Dlg3</i> RT-qPCR primer sequence	Eurofins Genomics	N/A	sense 5'-GAGCCAGTGACACGACAAGA-3'; antisense 5'-GCGGGAACCTCAGAGATGAGG-3'
Sequence-based reagent	<i>M. musculus Dlg4</i> RT-qPCR primer sequence	Eurofins Genomics	N/A	sense 5'-GGGCCTAAAGGACTTGGCTT-3'; antisense 5'-TGACATCCTCTAGCCCCACA-3'
Sequence-based reagent	<i>Rattus norvegicus Dlg1</i> PCR primer	Eurofins Genomics	rDLG1.kpnI	5'-CCGGTACCCCGGTCCGG AAGCAAGATAC-3'
Sequence-based reagent	<i>Rattus norvegicus Dlg1</i> PCR primer	Eurofins Genomics	rDLG1.notI	5'-CCGCGGCCGCTCATAATT

reagent				TTTCTTTTGCTGGGACCC AG -3'
DNA plasmid	pSpCas9(BB)-2A-Puro (PX459) V2.0	Addgene	Cat. #62988, pSpCas9	Expression vector, CRISPR
DNA plasmid	gRNA 1/pSpCas9	This study	pSpCas9-gRNA 1	Expression vector, CRISPR
DNA plasmid	gRNA 2/pSpCas9	This study	pSpCas9-gRNA 2	Expression vector, CRISPR
DNA plasmid	gRNA 3/pSpCas9	This study	pSpCas9-gRNA 3	Expression vector, CRISPR
DNA plasmid	gRNA 4/pSpCas9	This study	pSpCas9-gRNA 4	Expression vector, CRISPR
DNA plasmid	<i>Mus musculus</i> SDCCAG3/pCMV6-Myc-DDK	Origene	Cat. #MR217984, FLAG-MYC-SDCCAG3	Expression vector
DNA plasmid	<i>Homo sapiens</i> IFT20/pcDNA5.1-6xHis-3xFLAG-TEV	Made by Michael Tascher from Esben Lorentzen's lab using standard approaches as in ⁵⁶	HFT-IFT20	Expression vector
DNA plasmid	pEGFP-C1	Clontech	eGFP	Expression vector
DNA plasmid	<i>Mus musculus</i> IFT20/ pEGFP-N1	¹³	IFT20-eGFP	Expression vector
DNA plasmid	<i>Rattus norvegicus</i> DLG1/pEGFP-C1	⁹⁰	eGFP-DLG1	Expression vector, DLG1 insert is isolated from rat brain ⁹¹
DNA plasmid	pENTR220-mCherry-C1	⁹¹	N/A	Gateway entry vector
DNA plasmid	pCDH-EF1a-Gateway-IRES-BLAST	⁹¹	pCHD	Gateway destination vector for generating lentiviral expression vector
DNA plasmid	pMD2.G	⁹⁶	N/A	Lentiviral packaging vector
DNA plasmid	pCMVΔ-R8.2	⁹⁶	N/A	Lentiviral packaging vector
DNA plasmid	<i>Rattus norvegicus</i> DLG1/pENTR220-mCherry-C1	This study	pENTR220-mCherry-DLG1	Gateway entry vector, cloned in KpnI and NotI sites
DNA plasmid	<i>Rattus norvegicus</i> mCherry-DLG1/pCDH-EF1a-Gateway-IRES-BLAST	This study	pCDH-mCherry-DLG1	Lentiviral expression vector, generated with Gateway LR reaction using pENTR220-mCherry-DLG1 and pCDH plasmids
DNA plasmid	<i>Rattus norvegicus</i> mCherry-	This study	pCDH-mCherry-	Lentiviral expression vector, Generated by GenScript

	DLG1 ^{T507R} / pCDH-EF1a- Gateway-IRES- BLAST		DLG1 ^{T507R}	
Antibody	Anti-alpha- tubulin (mouse monoclonal)	Sigma-Aldrich	Cat. #T5168	WB (1:10000)
Antibody	Anti-acetylated alpha-tubulin (mouse monoclonal)	Sigma-Aldrich	Cat. #T7451	IFM (1:2000) IHC (1:2000)
Antibody	Anti-acetylated alpha-tubulin (rabbit monoclonal)	Abcam	Cat. #ab179484	IFM (1:2000)
Antibody	Anti-ARL13B (rabbit polyclonal)	Proteintech	Cat. #17711- 1-AP	IFM (1:500)
Antibody	Anti-DLG1 (rabbit polyclonal)	Abcam	Cat. #ab300481	IFM (1:750) WB (1:1000)
Antibody	Anti-DLG1 (rabbit polyclonal)	Thermo Scientific	Cat. #PA1- 741	WB (1:600)
Antibody	Anti-E-Cadherin (rabbit polyclonal)	Cell Signaling Technology	Cat. # 3195	IFM (1:1000)
Antibody	Anti-FLAG (mouse monoclonal)	Sigma-Aldrich	Cat. #F1804	WB (1:1000)
Antibody	Anti-GAPDH (rabbit polyclonal)	Cell Signaling Technology	Cat. #2118	WB (1:1000)
Antibody	Anti-GFP (chicken polyclonal)	Abcam	Cat. #ab13970	WB (1:1000)
Antibody	Anti-GFP (rabbit polyclonal)	Sigma-Aldrich	Cat. #SAB430113 8	WB (1:500)
Antibody	Anti-IFT20 (rabbit polyclonal)	Proteintech	Cat. #13615- 1-AP	IFM (1:200) IHC (1:100) WB (1:500)
Antibody	Anti-PALS1 (mouse monoclonal)	Santa Cruz Biotechnology	Cat. #sc- 365411	IFM (1:1000)
Antibody	Anti-PC2 (rabbit polyclonal)	PKD Research Resource Consortium	N/A	IFM (1:1000) WB (1:600)
Antibody	Anti-PC2 (mouse monoclonal)	Santa Cruz Biotechnology	Cat. #sc- 28331	IFM (1:500) WB (1:1000)
Antibody	Anti-SDCCAG3 (rabbit polyclonal)	Proteintech	Cat. #15969- 1-AP	IFM (1:600) IHC (1:100) WB (1:1000)

Antibody	Anti-SMAD2 (rabbit polyclonal)	Cell Signaling Technology	Cat. #5339	WB (1:200)
Antibody	Anti-pSMAD2 ^{Ser465/467} (rabbit polyclonal)	Cell Signaling Technology	Cat. #3108	WB (1:200)
Antibody	Anti-rSEC8 (mouse monoclonal)	Enzo Life Sciences	Cat. #ADI-VAM-SV016	IFM (1:1000) WB (1:2000)
Antibody	Anti-TAK1 (rabbit polyclonal)	Cell Signaling Technology	Cat. #4505	WB (1:300)
Antibody	Anti-pTAK1 ^{Ser412} (mouse monoclonal)	Bioss Antibodies	Cat. #bs-3435R	WB (1:200)
Antibody	Anti-pTAK1 ^{Thr184/187} (mouse monoclonal)	Bioss Antibodies	Cat. #bs-3439R	WB (1:200)
Antibody	Anti-Mouse-AF488 (donkey polyclonal)	Invitrogen	Cat. #A-21202	IFM (1:600)
Antibody	Anti-Mouse-AF568 (donkey polyclonal)	Invitrogen	Cat. # A-10037	IFM (1:600)
Antibody	Anti-Rabbit-AF488 (donkey polyclonal)	Invitrogen	Cat. # A-21206	IFM (1:600)
Antibody	Anti-Rabbit-AF568 (donkey polyclonal)	Invitrogen	Cat. #A-10042	IFM (1:600)
Antibody	Anti-Chicken-HRP (goat polyclonal)	Invitrogen	Cat. #A-16054	WB (1:6000)
Antibody	Anti-Mouse-HRP (goat polyclonal)	Agilent Technologies, Inc.	Cat. #P0447	WB (1:10000)
Antibody	Anti-Rabbit-HRP (swine polyclonal)	Agilent Technologies, Inc.	Cat. #P0399	WB (1:10000)
Peptide inhibitor	DLG-specific inhibitor	WuXi ApTtec (Shanghai, China)	AVLX-144	ReTat-N-dimer; described in ^{47,48}
Peptide inhibitor	DLG-specific inhibitor	WuXi ApTtec (Shanghai, China)	Tat-N-dimer	Described in ^{47,48}
Peptide inhibitor	non-PDZ-binding control	WuXi AppTec (Shanghai, China)	AVLX-144-AA	Described in ^{47,48}

Secondary detection	Streptavidin, Alexa Fluor 488 Conjugate	Invitrogen	Cat. #S32354	IFM (1:1000)
Fluorescent stain	DAPI	Sigma Aldrich	Cat. #D9542	IFM (1:5000)

Table 1. Cell lines and reagents used in this study. N/A, not applicable; WB, western blot; IHC, immunohistochemistry.

Figure legends

Figure 1. Loss of *Dlg1* in mouse kidney cells leads to elongated cilia. (A) H&E staining of representative kidney sections from wildtype and *Pax3Cre-Dlg1^{F/F}* mice. (B, C) Immunofluorescence staining for cilia (acetylated tubulin, yellow) and quantification of ciliary length in kidney sections of wildtype and *Pax3Cre-Dlg1^{F/F}* mice. * denotes $P < 0.05$. (D) Western blot analysis of total cell lysates of the indicated mCCD cells lines using antibodies against DLG1 and GAPDH (loading control). Molecular mass markers are shown in kDa to the left. (E) Representative image of transwell filter-grown mCCD cell lines (mCh-DLG1: mCherry-DLG1). Cilia were visualized using acetylated tubulin antibody (AcTub, magenta), cell-cell contacts were visualized with E-cadherin antibody (green) and nuclei were stained with DAPI (blue). (F, G) Quantification of ciliary length (F) and frequency (G) in the indicated transwell filter-grown mCCD lines. Ciliary length and ciliation rate was measured using the fully automated MATLAB script. Graphs represent accumulated data from three individual experiments, and statistical analysis was performed using Mann-Whitney U test (unpaired, two-tailed). Error bars represent means \pm SD. **, $P < 0.01$; ****, $P < 0.0001$; ns, not statistically significant.

Figure 2. Analysis of cilia mass spectrometry results. (A) Volcano plot visualizing differential protein expression in the ciliary proteome upon disruption of DLG1. The proteins are colored according to their significance tier (Tier 1, 2, 3, and non-significant (NS)). The total amount of affected candidate ciliary proteins found in Tier 1 upon *Dlg1* depletion are highlighted on the right side of the volcano plot, while the proteins related to this research are marked on the volcano plot. The complete list of identified proteins can be found in Supplementary Table S1. (B, C) Gene Ontology enrichment analysis for biological process (B) and cellular component (C) using the proteins found in Tier1. The tables show the top 15

terms that are significantly enriched (Fisher's exact test value ≤ 0.05) and are listed in order of their enrichment ratio along with the corresponding GO terms.

Figure 3. Loss of DLG1 impairs ciliary localization of SDCCAG3 in IMCD3 and mCCD cells.

(A, E) IFM analysis of ciliated cilia-BioID2 IMCD3 (A) and mCCD (E) cell lines showing comparative SDCCAG3 staining (green) in WT, *Dlg1*^{-/-} and mCherry-DLG1 (mCh-DLG1) rescue cells. Cilia were stained with antibodies against acetylated α -tubulin (AcTub, magenta), and nuclei visualized with DAPI staining (blue). Insets show enlarged images of cilia, asterisks mark the ciliary base. The merged insets show primary cilia with channels shifted to aid visualization. (B, F) Quantification of the relative mean fluorescence intensity (MFI) of SDCCAG3 staining along the cilium of cilia-BioID2 IMCD3 cell lines (B) or at the ciliary base of mCCD cell lines (F). Graphs represent WT normalized and accumulated data (n=3). Kruskal-Wallis test with Dunn's multiple comparison test was used for the statistical analysis. Data are shown as mean \pm SD. ****, $P < 0.0001$. (C, D, G) Western blot analysis of total cell lysates of cilia-BioID2 IMCD3 (C, D) or mCCD (G) cell lines. Blots were probed with antibodies as indicated, GAPDH was used as loading control. Molecular mass markers are shown in kDa to the left.

Figure 4. Conditional loss of DLG1 in mouse kidney leads to impaired ciliary localization of SDCCAG3 and IFT20.

(A, B) Immunofluorescence staining of SDCCAG3 (A) or IFT20 (B), both in yellow, and acetylated α -tubulin (AcTub, magenta) in kidney sections from wildtype and *Pax3Cre-Dlg1*^{F/F} mice. (C) Quantification of relative MFI of SDCCAG3 and IFT20 in cilia of wildtype and *Pax3Cre-Dlg1*^{F/F} mice, respectively. * denotes $P < 0.05$.

Figure 5. Loss of DLG1 affects ciliary composition in transwell filter-grown mCCD cells.

(A, B) Representative top (A) and side view (B) confocal images of transwell filter-

grown WT, *Dlg1*^{-/-} and mCh-DLG1 rescue mCCD cell lines. The cells were stained for E-cadherin (green) and PALS1 (magenta) to visualize the basolateral membrane and apical-lateral border, respectively. (C, E) IFM analysis of PC2 (C) or SDCCAG3 (E) (green) in transwell filter-grown mCCD cell lines. Cilia were visualized with antibody against acetylated tubulin (AcTub, magenta), and nuclei stained with DAPI (blue). Insets show enlarged images of cilia, while the merged insets show primary cilia with channels shifted to aid visualization. (D, F) Quantification of the relative MFI of PC2 (D) and SDCCAG3 (F) along the cilium (right panels) and at the ciliary base (left panels). The graphs represent normalized and accumulated data (n=3). The number of dots in each condition represents the number of primary cilia quantified. The MFI of SDCCAG3 or PC2 was measured using the fully automated MATLAB-based quantification. Statistical analysis utilized one-way ANOVA with Tukey's multiple comparison test. Data are shown as mean ± SD. ****, P<0.0001.

Figure 6. A CAKUT-associated DLG1 missense variant fails to rescue ciliary phenotype of *Dlg1*^{-/-} mCCD cells. (A) DLG1 protein domain structure and schematic representation and localization of the human CAKUT-associated DLG1^{T489R} variant and the rat counterpart (DLG1^{T507R}). (B) Western blot validation of stable expression of transgenic mutant mCherry-DLG1 (mCh-DLG1^{T507R}) in mCCD cells using antibodies as indicated. (C, F) Quantification of relative MFI of SDCCAG3 (C) and IFT20 (F) at the ciliary base of indicated mCCD cell lines, based on images as shown in panels (D) and (E), respectively. Kruskal-Wallis test with Dunn's multiple comparison test was used for statistical analysis. Data are shown as mean ± SD (n=3). *, P<0.05; ***, P<0.001; ****, P<0.0001. In (D, E) ciliated mCCD WT and *Dlg1*^{-/-} and mCherry-DLG1 rescue cells were analyzed by IFM with antibodies against SDCCAG3 (D) or IFT20 (E), both shown in green. Acetylated α-tubulin (AcTub, magenta) was used to stain cilia; nuclei were visualized with DAPI (blue). Insets show enlarged images of cilia,

asterisks mark the ciliary base. The merged insets show primary cilia with channels shifted to aid visualization. **(G, I)** Western blot analysis of total or phosphorylated (p) SMAD2 **(G)** and TAK1 **(I)** upon stimulation with TGF β -2 ligand for indicated times in growth-arrested mCCD cells. **(H, J)** Quantifications of protein phosphorylation shown in panels **(G, I)**, respectively. Error bars represent means \pm SD (n = 3).

Figure 7. Physical interactions between, DLG1, IFT20 and SDCCAG3. **(A, B)** Immunoprecipitation with anti-GFP beads was performed in HEK293T cells transiently expressing FLAG-SDCCAG3 **(A)** or FLAG-IFT20 **(B)** together with the indicated GFP-fusions. Input and pellet fractions were subjected to SDS-PAGE and western blot analysis using antibodies against FLAG or GFP, as indicated, and GFP expressed alone was used as negative control. Molecular mass markers are indicated in kDa to the left. **(C)** Structural prediction for the complex between MmSDCCAG3 (yellow) and MmIFT20 (cyan) in cartoon representation (upper panel). The structure is predicted to be an anti-parallel hetero-dimer coiled coil. The lower panel includes IFT54 showing its binding to IFT20 is mutually exclusive with binding of SDCCAG3 to IFT20. **(D)** Proposed model for how DLG1 promotes ciliary trafficking of SDCCAG3, IFT20 and PC2. Based on ^{7,9} and data presented in the current study. CRE, common recycling endosome.

References

- 1 Mill, P., Christensen, S. T. & Pedersen, L. B. Primary cilia as dynamic and diverse signalling hubs in development and disease. *Nat Rev Genet* **24**, 421-441, doi:10.1038/s41576-023-00587-9 (2023).

- 2 Pazour, G. J., San Agustin, J. T., Follit, J. A., Rosenbaum, J. L. & Witman, G. B. Polycystin-2 localizes to kidney cilia and the ciliary level is elevated in orpk mice with polycystic kidney disease. *Curr Biol* **12**, R378-380 (2002).
- 3 Yoder, B. K., Hou, X. & Guay-Woodford, L. M. The Polycystic Kidney Disease Proteins, Polycystin-1, Polycystin-2, Polaris, and Cystin, Are Co-Localized in Renal Cilia. *Journal of the American Society of Nephrology* **13**, 2508-2516, doi:10.1097/01.asn.0000029587.47950.25 (2002).
- 4 Ma, M., Gallagher, A. R. & Somlo, S. Ciliary Mechanisms of Cyst Formation in Polycystic Kidney Disease. *Cold Spring Harb Perspect Biol* **9**, doi:10.1101/cshperspect.a028209 (2017).
- 5 Cantero, M. D. R. & Cantiello, H. F. Polycystin-2 (TRPP2): Ion channel properties and regulation. *Gene* **827**, 146313, doi:10.1016/j.gene.2022.146313 (2022).
- 6 Walker, R. V. *et al.* Ciliary exclusion of Polycystin-2 promotes kidney cystogenesis in an autosomal dominant polycystic kidney disease model. *Nat Commun* **10**, 4072, doi:10.1038/s41467-019-12067-y (2019).
- 7 Monis, W. J., Faundez, V. & Pazour, G. J. BLOC-1 is required for selective membrane protein trafficking from endosomes to primary cilia. *J Cell Biol* **216**, 2131-2150, doi:10.1083/jcb.201611138 (2017).
- 8 Nachury, M. V. The molecular machines that traffic signaling receptors into and out of cilia. *Current Opinion in Cell Biology* **51**, 124-131, doi:10.1016/j.ceb.2018.03.004 (2018).
- 9 Hu, J. & Harris, P. C. Regulation of polycystin expression, maturation and trafficking. *Cell Signal* **72**, 109630, doi:10.1016/j.cellsig.2020.109630 (2020).

- 10 Stoops, E. H. & Caplan, M. J. Trafficking to the apical and basolateral membranes in polarized epithelial cells. *J Am Soc Nephrol* **25**, 1375-1386, doi:10.1681/ASN.2013080883 (2014).
- 11 Hoffmeister, H. *et al.* Polycystin-2 takes different routes to the somatic and ciliary plasma membrane. *J Cell Biol* **192**, 631-645, doi:10.1083/jcb.201007050 (2011).
- 12 Kim, H. *et al.* Ciliary membrane proteins traffic through the Golgi via a Rabep1/GGA1/Arl3-dependent mechanism. *Nat Commun* **5**, 5482, doi:10.1038/ncomms6482 (2014).
- 13 Follit, J. A., Tuft, R. A., Fogarty, K. E. & Pazour, G. J. The intraflagellar transport protein IFT20 is associated with the Golgi complex and is required for cilia assembly. *Mol Biol Cell* **17**, 3781-3792 (2006).
- 14 Follit, J. A. *et al.* The Golgin GMAP210/TRIP11 anchors IFT20 to the Golgi complex. *PLoS Genet* **4**, e1000315, doi:10.1371/journal.pgen.1000315 (2008).
- 15 Yu, F., Sharma, S., Skowronek, A. & Erdmann, K. S. The serologically defined colon cancer antigen-3 (SDCCAG3) is involved in the regulation of ciliogenesis. *Sci Rep* **6**, 35399, doi:10.1038/srep35399 (2016).
- 16 Tilley, F. C. *et al.* Retromer associates with the cytoplasmic amino-terminus of polycystin-2. *J Cell Sci* **131**, doi:10.1242/jcs.211342 (2018).
- 17 Funke, L., Dakoji, S. & Brecht, D. S. Membrane-associated guanylate kinases regulate adhesion and plasticity at cell junctions. *Annu Rev Biochem* **74**, 219-245, doi:10.1146/annurev.biochem.74.082803.133339 (2005).
- 18 Lickert, H. & Van Campenhout, C. A. Evolution of the Discs large gene family provides new insights into the establishment of apical epithelial polarity and the etiology of mental retardation. *Commun Integr Biol* **5**, 287-290, doi:10.4161/cib.19792 (2012).

- 19 Mauceri, D., Gardoni, F., Marcello, E. & Di Luca, M. Dual role of CaMKII-dependent SAP97 phosphorylation in mediating trafficking and insertion of NMDA receptor subunit NR2A. *J Neurochem* **100**, 1032-1046, doi:10.1111/j.1471-4159.2006.04267.x (2007).
- 20 Gardoni, F. *et al.* SAP97 directs the localization of Kv4.2 to spines in hippocampal neurons: regulation by CaMKII. *J Biol Chem* **282**, 28691-28699, doi:10.1074/jbc.M701899200 (2007).
- 21 Tiffany, A. M. *et al.* PSD-95 and SAP97 exhibit distinct mechanisms for regulating K(+) channel surface expression and clustering. *J Cell Biol* **148**, 147-158, doi:10.1083/jcb.148.1.147 (2000).
- 22 Sans, N. *et al.* Synapse-associated protein 97 selectively associates with a subset of AMPA receptors early in their biosynthetic pathway. *J Neurosci* **21**, 7506-7516, doi:10.1523/JNEUROSCI.21-19-07506.2001 (2001).
- 23 van Ree, J. H., Nam, H. J., Jeganathan, K. B., Kanakkanthara, A. & van Deursen, J. M. Pten regulates spindle pole movement through Dlg1-mediated recruitment of Eg5 to centrosomes. *Nat Cell Biol* **18**, 814-821, doi:10.1038/ncb3369 (2016).
- 24 Mick, D. U. *et al.* Proteomics of Primary Cilia by Proximity Labeling. *Dev Cell* **35**, 497-512, doi:10.1016/j.devcel.2015.10.015 (2015).
- 25 Kohli, P. *et al.* The ciliary membrane-associated proteome reveals actin-binding proteins as key components of cilia. *EMBO Rep* **18**, 1521-1535, doi:10.15252/embr.201643846 (2017).
- 26 Datta, P. *et al.* Accumulation of non-outer segment proteins in the outer segment underlies photoreceptor degeneration in Bardet-Biedl syndrome. *Proc Natl Acad Sci U S A* **112**, E4400-4409, doi:10.1073/pnas.1510111112 (2015).

- 27 Hanada, T., Lin, L., Tibaldi, E. V., Reinherz, E. L. & Chishti, A. H. GAKIN, a novel kinesin-like protein associates with the human homologue of the Drosophila discs large tumor suppressor in T lymphocytes. *J Biol Chem* **275**, 28774-28784, doi:10.1074/jbc.M000715200 (2000).
- 28 Schou, K. B. *et al.* KIF13B establishes a CAV1-enriched microdomain at the ciliary transition zone to promote Sonic hedgehog signaling. *Nature Communications* **8**, 14177, doi:10.1038/NCOMMS14177 (2017).
- 29 Juhl, A. D. *et al.* Transient accumulation and bidirectional movement of KIF13B in primary cilia. *J Cell Sci* **136**, doi:10.1242/jcs.259257 (2023).
- 30 Caruana, G. & Bernstein, A. Craniofacial dysmorphogenesis including cleft palate in mice with an insertional mutation in the discs large gene. *Mol Cell Biol* **21**, 1475-1483, doi:10.1128/MCB.21.5.1475-1483.2001 (2001).
- 31 Mahoney, Z. X. *et al.* Discs-large homolog 1 regulates smooth muscle orientation in the mouse ureter. *Proc Natl Acad Sci U S A* **103**, 19872-19877, doi:10.1073/pnas.0609326103 (2006).
- 32 Iizuka-Kogo, A., Ishidao, T., Akiyama, T. & Senda, T. Abnormal development of urogenital organs in *Dlgh1*-deficient mice. *Development* **134**, 1799-1807, doi:10.1242/dev.02830 (2007).
- 33 Westland, R. *et al.* Copy number variation analysis identifies novel CAKUT candidate genes in children with a solitary functioning kidney. *Kidney Int* **88**, 1402-1410, doi:10.1038/ki.2015.239 (2015).
- 34 Nicolaou, N., Renkema, K. Y., Bongers, E. M., Giles, R. H. & Knoers, N. V. Genetic, environmental, and epigenetic factors involved in CAKUT. *Nat Rev Nephrol* **11**, 720-731, doi:10.1038/nrneph.2015.140 (2015).

- 35 Willatt, L. *et al.* 3q29 microdeletion syndrome: clinical and molecular characterization of a new syndrome. *Am J Hum Genet* **77**, 154-160, doi:10.1086/431653 (2005).
- 36 Kim, S. T., Ahn, S. Y., Swat, W. & Miner, J. H. DLG1 influences distal ureter maturation via a non-epithelial cell autonomous mechanism involving reduced retinoic acid signaling, Ret expression, and apoptosis. *Dev Biol* **390**, 160-169, doi:10.1016/j.ydbio.2014.03.014 (2014).
- 37 Montesano, R., Ghzili, H., Carrozzino, F., Rossier, B. C. & Feraille, E. cAMP-dependent chloride secretion mediates tubule enlargement and cyst formation by cultured mammalian collecting duct cells. *Am J Physiol Renal Physiol* **296**, F446-457, doi:10.1152/ajprenal.90415.2008 (2009).
- 38 Pedersen, L. B., Schrøder, J. M., Satir, P. & Christensen, S. T. The ciliary cytoskeleton. *Comprehensive Physiology* **2**, 779-803 (2012).
- 39 Avasthi, P. & Marshall, W. F. Stages of ciliogenesis and regulation of ciliary length. *Differentiation* **83**, S30-42, doi:10.1016/j.diff.2011.11.015 (2012).
- 40 Aslanyan, M. G. *et al.* A targeted multi-proteomics approach generates a blueprint of the ciliary ubiquitinome. *Frontiers in Cell and Developmental Biology* **11**, doi:10.3389/fcell.2023.1113656 (2023).
- 41 McGough, I. J. *et al.* Identification of molecular heterogeneity in SNX27-retromer-mediated endosome-to-plasma-membrane recycling. *J Cell Sci* **127**, 4940-4953, doi:10.1242/jcs.156299 (2014).
- 42 Cole, D. G. *et al.* *Chlamydomonas* kinesin-II-dependent intraflagellar transport (IFT): IFT particles contain proteins required for ciliary assembly in *Caenorhabditis elegans* sensory neurons. *J Cell Biol* **141**, 993-1008 (1998).

- 43 Inoue, M., Chiang, S. H., Chang, L., Chen, X. W. & Saltiel, A. R. Compartmentalization of the exocyst complex in lipid rafts controls Glut4 vesicle tethering. *Mol Biol Cell* **17**, 2303-2311, doi:10.1091/mbc.e06-01-0030 (2006).
- 44 Bolis, A. *et al.* Dlg1, Sec8, and Mtmr2 regulate membrane homeostasis in Schwann cell myelination. *The Journal of neuroscience : the official journal of the Society for Neuroscience* **29**, 8858-8870, doi:10.1523/JNEUROSCI.1423-09.2009 (2009).
- 45 Fogelgren, B. *et al.* The exocyst protein Sec10 interacts with Polycystin-2 and knockdown causes PKD-phenotypes. *PLoS Genet* **7**, e1001361, doi:10.1371/journal.pgen.1001361 (2011).
- 46 Seixas, C. *et al.* Arl13b and the exocyst interact synergistically in ciliogenesis. *Mol Biol Cell* **27**, 308-320, doi:10.1091/mbc.E15-02-0061 (2016).
- 47 Bach, A. *et al.* A high-affinity, dimeric inhibitor of PSD-95 bivalently interacts with PDZ1-2 and protects against ischemic brain damage. *Proc Natl Acad Sci U S A* **109**, 3317-3322, doi:10.1073/pnas.1113761109 (2012).
- 48 Bach, A. *et al.* Modified Peptides as Potent Inhibitors of the Postsynaptic Density-95/N-Methyl-d-Aspartate Receptor Interaction. *Journal of Medicinal Chemistry* **51**, 6450-6459, doi:10.1021/jm800836w (2008).
- 49 Unno, K., Hanada, T. & Chishti, A. H. Functional involvement of human discs large tumor suppressor in cytokinesis. *Exp Cell Res* **314**, 3118-3129, doi:10.1016/j.yexcr.2008.07.032 (2008).
- 50 Bernabe-Rubio, M. *et al.* Novel role for the midbody in primary ciliogenesis by polarized epithelial cells. *J Cell Biol* **214**, 259-273, doi:10.1083/jcb.201601020 (2016).

- 51 Choi, M. E., Ding, Y. & Kim, S. I. TGF-beta signaling via TAK1 pathway: role in kidney fibrosis. *Semin Nephrol* **32**, 244-252, doi:10.1016/j.semnephrol.2012.04.003 (2012).
- 52 Sureshababu, A., Muhsin, S. A. & Choi, M. E. TGF-beta signaling in the kidney: profibrotic and protective effects. *Am J Physiol Renal Physiol* **310**, F596-F606, doi:10.1152/ajprenal.00365.2015 (2016).
- 53 Clement, C. A. *et al.* Regulation of TGF β signaling by endocytosis at the pocket region of the primary cilium *Cell Rep* **3**, 1806-1814 (2013).
- 54 Christensen, S. T., Morthorst, S. K., Mogensen, J. B. & Pedersen, L. B. Primary Cilia and Coordination of Receptor Tyrosine Kinase (RTK) and Transforming Growth Factor beta (TGF-beta) Signaling. *Cold Spring Harb Perspect Biol* **9**, a028167, doi:10.1101/cshperspect.a028167 (2017).
- 55 Jumper, J. *et al.* Highly accurate protein structure prediction with AlphaFold. *Nature* **596**, 583-589, doi:10.1038/s41586-021-03819-2 (2021).
- 56 Taschner, M. *et al.* Intraflagellar transport proteins 172, 80, 57, 54, 38, and 20 form a stable tubulin-binding IFT-B2 complex. *EMBO J* **35**, 773-790, doi:10.15252/embj.201593164 (2016).
- 57 Nazarian, R., Starcevic, M., Spencer, M. J. & Dell'Angelica, E. C. Reinvestigation of the dysbindin subunit of BLOC-1 (biogenesis of lysosome-related organelles complex-1) as a dystrobrevin-binding protein. *Biochem J* **395**, 587-598, doi:10.1042/BJ20051965 (2006).
- 58 Kanai, Y., Wang, D. & Hirokawa, N. KIF13B enhances the endocytosis of LRP1 by recruiting LRP1 to caveolae. *J Cell Biol* **204**, 395-408, doi:10.1083/jcb.201309066 (2014).

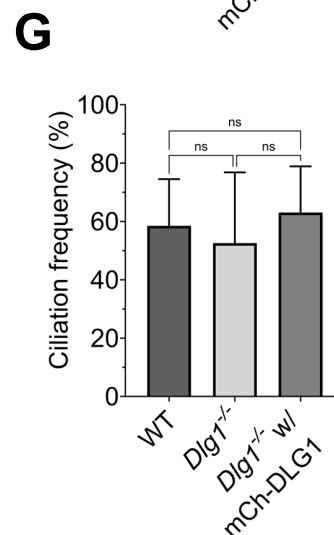
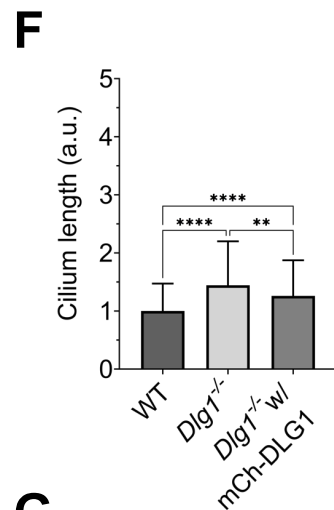
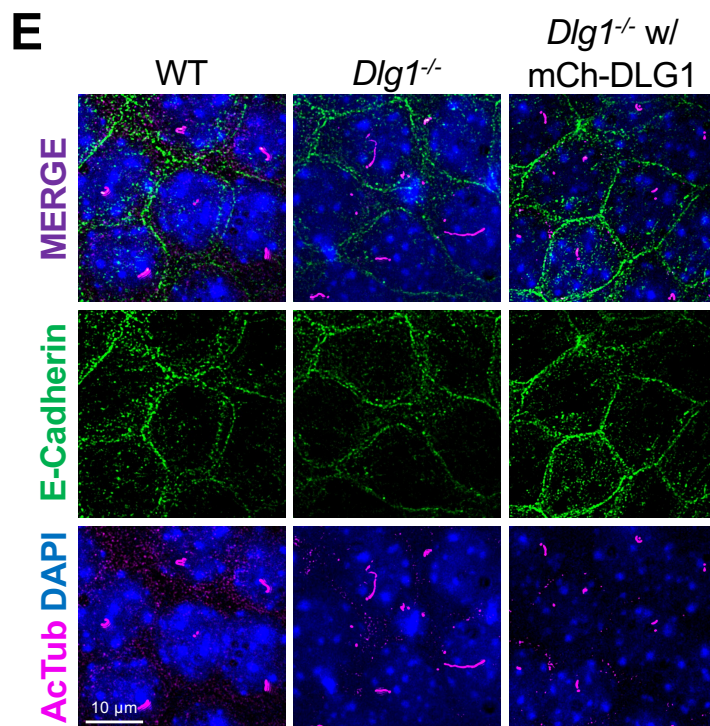
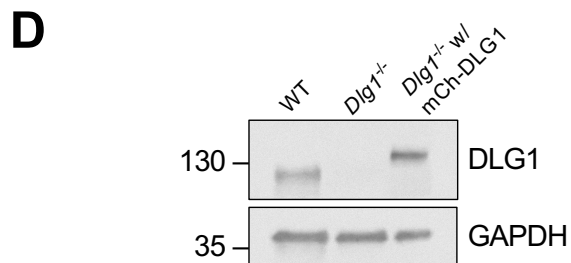
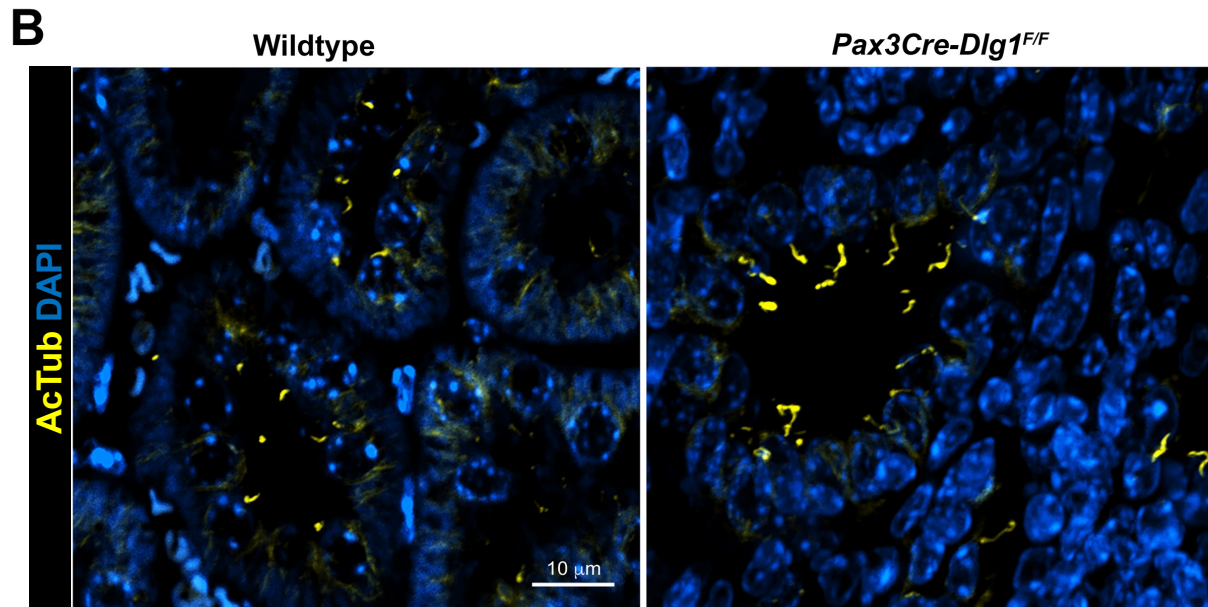
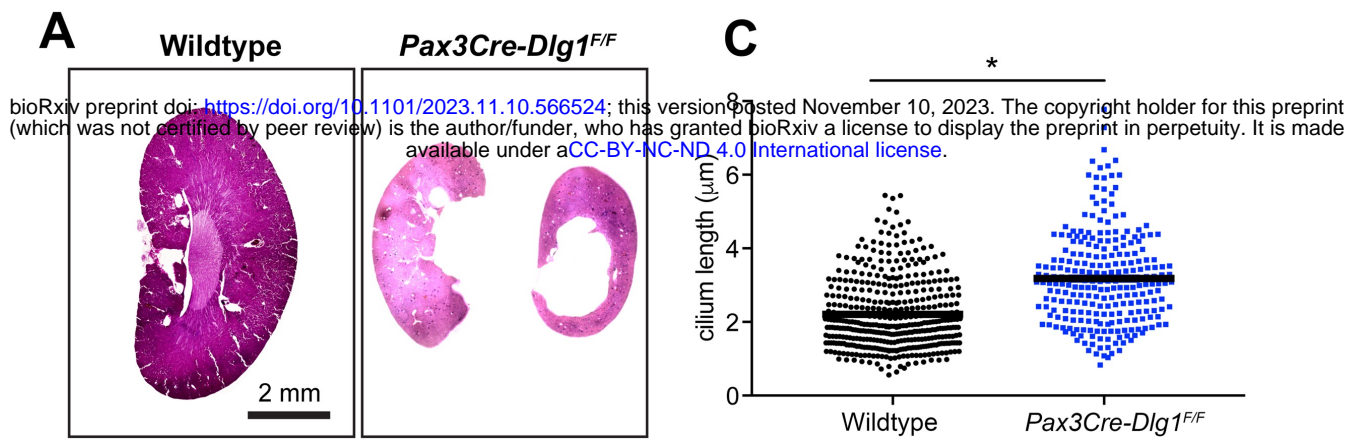
- 59 Morthorst, S. K. *et al.* Angiotensin isoform 2 promotes binding of PALS1 to KIF13B at the base of primary cilia and suppresses ciliary elongation. *bioRxiv*, 2021.2010.2014.464392, doi:10.1101/2021.10.14.464392 (2022).
- 60 Huttlin, E. L. *et al.* Dual proteome-scale networks reveal cell-specific remodeling of the human interactome. *Cell* **184**, 3022-3040 e3028, doi:10.1016/j.cell.2021.04.011 (2021).
- 61 Shao, L. *et al.* Genetic reduction of cilium length by targeting intraflagellar transport 88 protein impedes kidney and liver cyst formation in mouse models of autosomal polycystic kidney disease. *Kidney Int* **98**, 1225-1241, doi:10.1016/j.kint.2020.05.049 (2020).
- 62 Mochizuki, T. *et al.* PKD2, a gene for polycystic kidney disease that encodes an integral membrane protein. *Science* **272**, 1339-1342, doi:10.1126/science.272.5266.1339 (1996).
- 63 Heider, M. R. & Munson, M. Exorcising the exocyst complex. *Traffic* **13**, 898-907, doi:10.1111/j.1600-0854.2012.01353.x (2012).
- 64 Bolis, A. *et al.* Dlg1, Sec8, and Mtmr2 regulate membrane homeostasis in Schwann cell myelination. *J Neurosci* **29**, 8858-8870, doi:10.1523/JNEUROSCI.1423-09.2009 (2009).
- 65 Yamanaka, T. & Ohno, S. Role of Lgl/Dlg/Scribble in the regulation of epithelial junction, polarity and growth. *Front Biosci* **13**, 6693-6707, doi:10.2741/3182 (2008).
- 66 Osterweil, E., Wells, D. G. & Mooseker, M. S. A role for myosin VI in postsynaptic structure and glutamate receptor endocytosis. *J Cell Biol* **168**, 329-338, doi:10.1083/jcb.200410091 (2005).

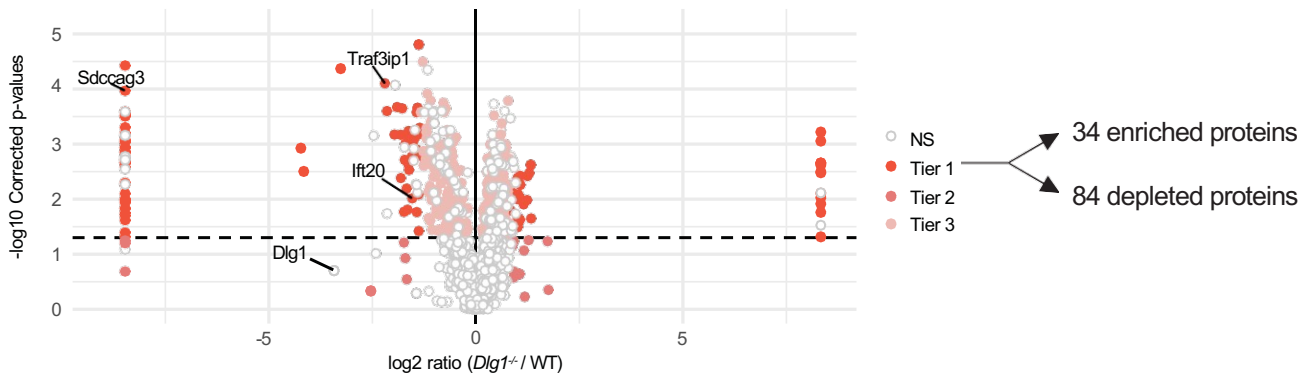
- 67 de Vreede, G. *et al.* The Scribble module regulates retromer-dependent endocytic trafficking during epithelial polarization. *Development* **141**, 2796-2802, doi:10.1242/dev.105403 (2014).
- 68 Wang, P. *et al.* SNX17 Recruits USP9X to Antagonize MIB1-Mediated Ubiquitination and Degradation of PCMI during Serum-Starvation-Induced Ciliogenesis. *Cells* **8**, doi:10.3390/cells8111335 (2019).
- 69 Severin, M. *et al.* Dynamic localization of the Na⁺-HCO₃⁻ co-transporter NBCn1 to the plasma membrane, centrosomes, spindle and primary cilia. *J Cell Sci* **136**, doi:10.1242/jcs.260687 (2023).
- 70 Olesen, C. W. *et al.* Trafficking, localization and degradation of the Na⁽⁺⁾,HCO₃⁽⁻⁾ co-transporter NBCn1 in kidney and breast epithelial cells. *Sci Rep* **8**, 7435, doi:10.1038/s41598-018-25059-7 (2018).
- 71 Mellman, I. & Nelson, W. J. Coordinated protein sorting, targeting and distribution in polarized cells. *Nat Rev Mol Cell Biol* **9**, 833-845, doi:10.1038/nrm2525 (2008).
- 72 Akhmanova, A. & Kapitein, L. C. Mechanisms of microtubule organization in differentiated animal cells. *Nat Rev Mol Cell Biol* **23**, 541-558, doi:10.1038/s41580-022-00473-y (2022).
- 73 Sang, L. *et al.* Mapping the NPHP-JBTS-MKS Protein Network Reveals Ciliopathy Disease Genes and Pathways. *Cell* **145**, 513-528, doi:10.1016/j.cell.2011.04.019 (2011).
- 74 Delous, M. *et al.* Nephrocystin-1 and nephrocystin-4 are required for epithelial morphogenesis and associate with PALS1/PATJ and Par6. *Hum Mol Genet* **18**, 4711-4723, doi:10.1093/hmg/ddp434 (2009).

- 75 Tan, B. *et al.* The Mammalian Crumbs Complex Defines a Distinct Polarity Domain Apical of Epithelial Tight Junctions. *Curr Biol* **30**, 2791-2804 e2796, doi:10.1016/j.cub.2020.05.032 (2020).
- 76 Fan, S. *et al.* Polarity proteins control ciliogenesis via kinesin motor interactions. *Curr Biol* **14**, 1451-1461 (2004).
- 77 Bazellieres, E., Aksenova, V., Barthelemy-Requin, M., Massey-Harroche, D. & Le Bivic, A. Role of the Crumbs proteins in ciliogenesis, cell migration and actin organization. *Semin Cell Dev Biol* **81**, 13-20, doi:10.1016/j.semcdb.2017.10.018 (2018).
- 78 Morthorst, S. K. *et al.* Angiotensin isoform 2 promotes binding of PALS1 to KIF13B at the base of primary cilia and suppresses ciliary elongation. *bioRxiv*, 2021.2010.2014.464392, doi:10.1101/2021.10.14.464392 (2021).
- 79 Duning, K. *et al.* Polycystin-2 activity is controlled by transcriptional coactivator with PDZ binding motif and PALS1-associated tight junction protein. *J Biol Chem* **285**, 33584-33588, doi:10.1074/jbc.C110.146381 (2010).
- 80 Kim, S. I. & Choi, M. E. TGF-beta-activated kinase-1: New insights into the mechanism of TGF-beta signaling and kidney disease. *Kidney Res Clin Pract* **31**, 94-105, doi:10.1016/j.krcp.2012.04.322 (2012).
- 81 Peng, Z. *et al.* Dlg1 Knockout Inhibits Microglial Activation and Alleviates Lipopolysaccharide-Induced Depression-Like Behavior in Mice. *Neurosci Bull* **37**, 1671-1682, doi:10.1007/s12264-021-00765-x (2021).
- 82 Podrini, C., Cassina, L. & Boletta, A. Metabolic reprogramming and the role of mitochondria in polycystic kidney disease. *Cell Signal* **67**, 109495, doi:10.1016/j.cellsig.2019.109495 (2020).

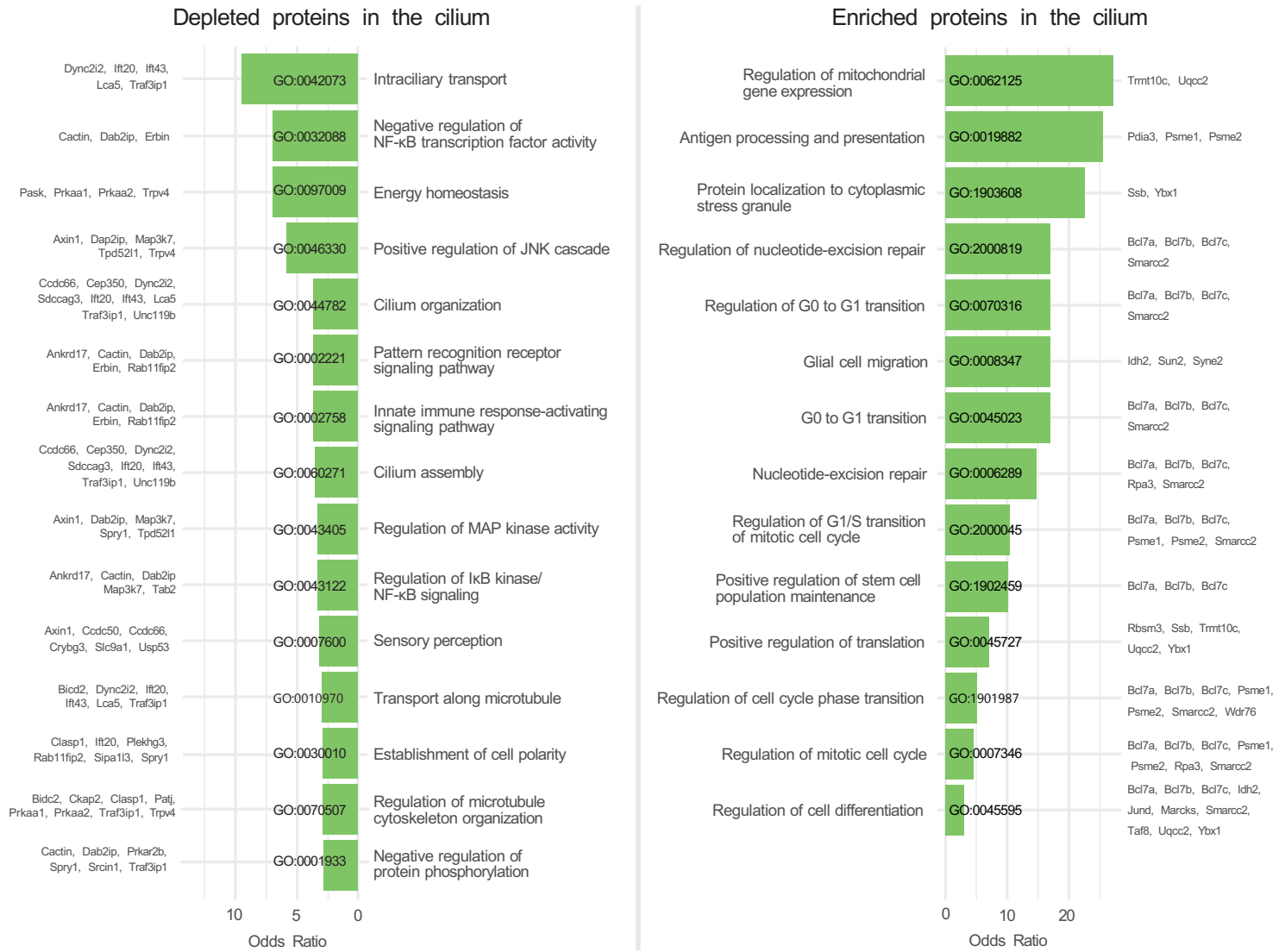
- 83 Steidl, M. E. *et al.* Primary cilia sense glutamine availability and respond via asparagine synthetase. *Nat Metab* **5**, 385-397, doi:10.1038/s42255-023-00754-6 (2023).
- 84 Walker, R. V. *et al.* Fibrocystin/Polyductin releases a C-terminal fragment that translocates into mitochondria and suppresses cystogenesis. *Nat Commun* **14**, 6513, doi:10.1038/s41467-023-42196-4 (2023).
- 85 Chong, Y. C., Mann, R. K., Zhao, C., Kato, M. & Beachy, P. A. Bifurcating action of Smoothed in Hedgehog signaling is mediated by Dlg5. *Genes Dev* **29**, 262-276, doi:10.1101/gad.252676.114 (2015).
- 86 Marquez, J. *et al.* DLG5 variants are associated with multiple congenital anomalies including ciliopathy phenotypes. *J Med Genet* **58**, 453-464, doi:10.1136/jmedgenet-2019-106805 (2021).
- 87 Lu, Q. *et al.* Early steps in primary cilium assembly require EHD1/EHD3-dependent ciliary vesicle formation. *Nat Cell Biol* **17**, 531, doi:10.1038/ncb3155 (2015).
- 88 Doench, J. G. *et al.* Optimized sgRNA design to maximize activity and minimize off-target effects of CRISPR-Cas9. *Nat Biotechnol* **34**, 184-191, doi:10.1038/nbt.3437 (2016).
- 89 Ran, F. A. *et al.* Genome engineering using the CRISPR-Cas9 system. *Nat Protoc* **8**, 2281-2308, doi:10.1038/nprot.2013.143 (2013).
- 90 Wu, H., Reuver, S. M., Kuhlendahl, S., Chung, W. J. & Garner, C. C. Subcellular targeting and cytoskeletal attachment of SAP97 to the epithelial lateral membrane. *J Cell Sci* **111** (Pt 16), 2365-2376, doi:10.1242/jcs.111.16.2365 (1998).
- 91 Campeau, E. *et al.* A versatile viral system for expression and depletion of proteins in mammalian cells. *PLoS One* **4**, e6529, doi:10.1371/journal.pone.0006529 (2009).

- 92 Tyanova, S. *et al.* The Perseus computational platform for comprehensive analysis of (prote)omics data. *Nat Methods* **13**, 731-740, doi:10.1038/nmeth.3901 (2016).
- 93 Alexa, A. & Rahnenfuhrer, J. topGO: Enrichment Analysis for Gene Ontology. *R package version 2.54.0*, doi:doi:10.18129/B9.bioc.topGO (2023).
- 94 Hua, K. & Ferland, R. J. Fixation methods can differentially affect ciliary protein immunolabeling. *Cilia* **6**, 5, doi:10.1186/s13630-017-0045-9 (2017).
- 95 He, K. *et al.* Axoneme polyglutamylation regulated by Joubert syndrome protein ARL13B controls ciliary targeting of signaling molecules. *Nat Commun* **9**, 3310, doi:10.1038/s41467-018-05867-1 (2018).
- 96 Goncalves, A. B. *et al.* CEP78 functions downstream of CEP350 to control biogenesis of primary cilia by negatively regulating CP110 levels. *Elife* **10**, doi:10.7554/eLife.63731 (2021).
- 97 Schindelin, J. *et al.* Fiji: an open-source platform for biological-image analysis. *Nat Methods* **9**, 676-682, doi:10.1038/nmeth.2019 (2012).
- 98 Evans, R. *et al.* Protein complex prediction with AlphaFold-Multimer. *bioRxiv*, 2021.2010.2004.463034, doi:10.1101/2021.10.04.463034 (2022).
- 99 Gaeggeler, H. P. *et al.* Mineralocorticoid versus glucocorticoid receptor occupancy mediating aldosterone-stimulated sodium transport in a novel renal cell line. *J Am Soc Nephrol* **16**, 878-891, doi:10.1681/ASN.2004121110 (2005).

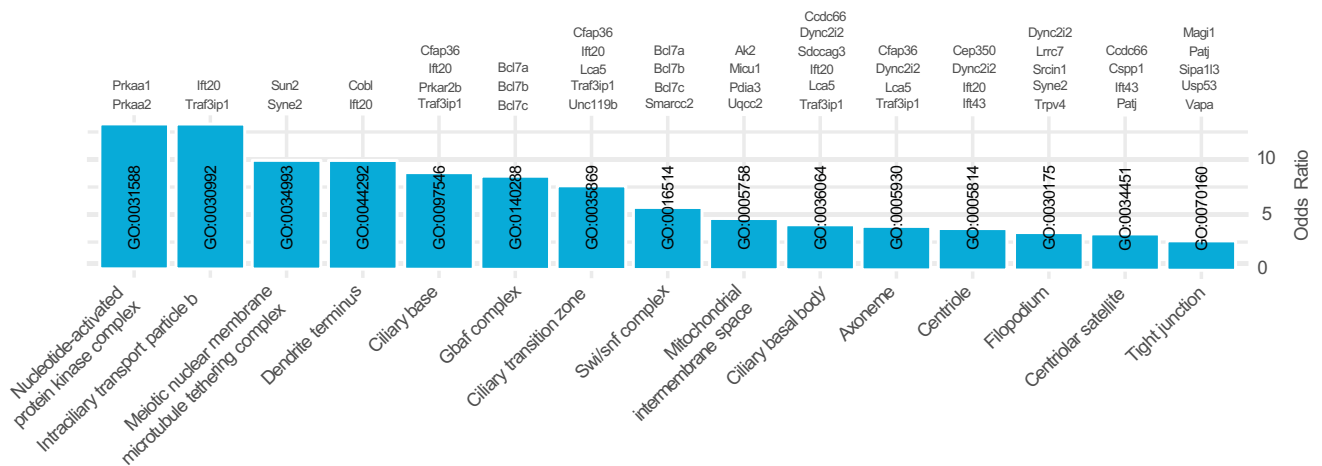


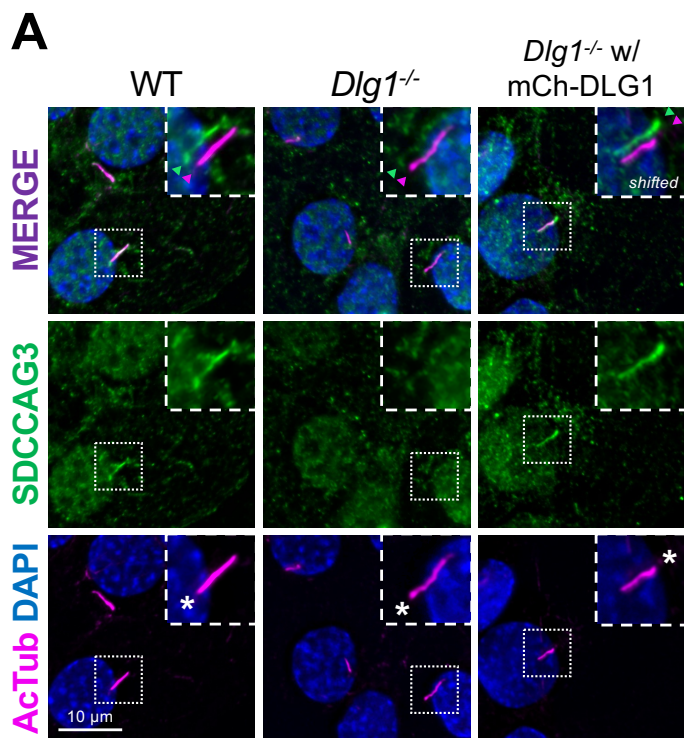
A**B**

Top 15 enriched GO Biological Process terms

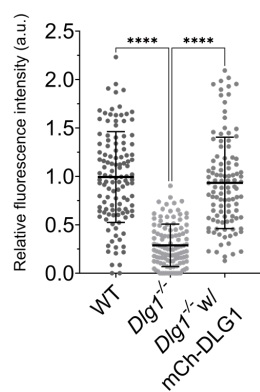
**C**

Top 15 enriched GO Cellular Component terms

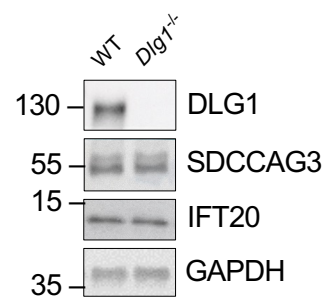




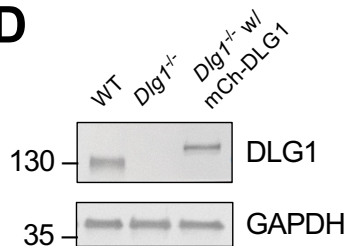
B Relative levels of SDCCAG3 along the cilium



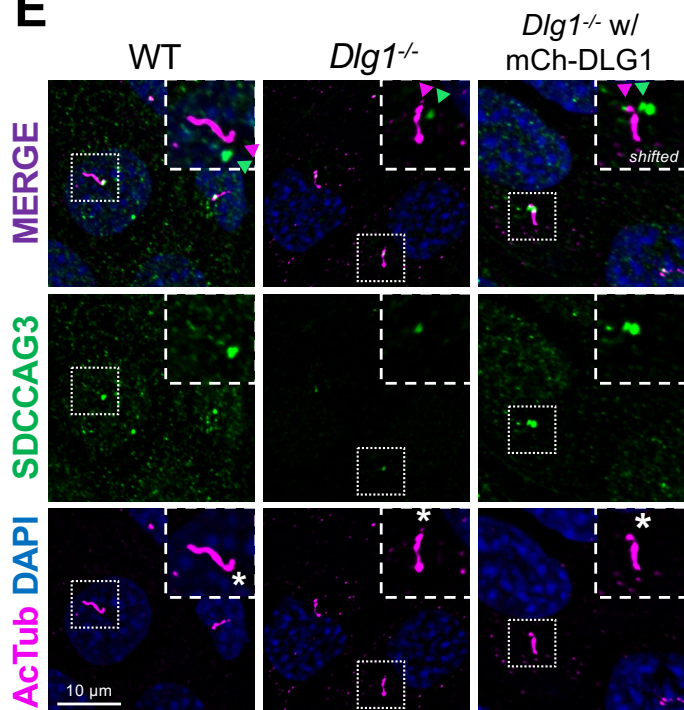
C



D

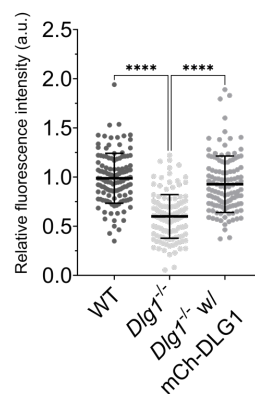


E

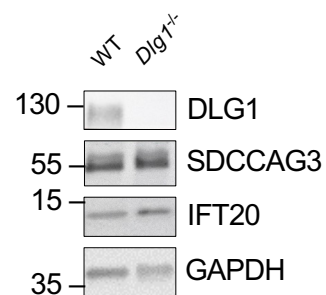


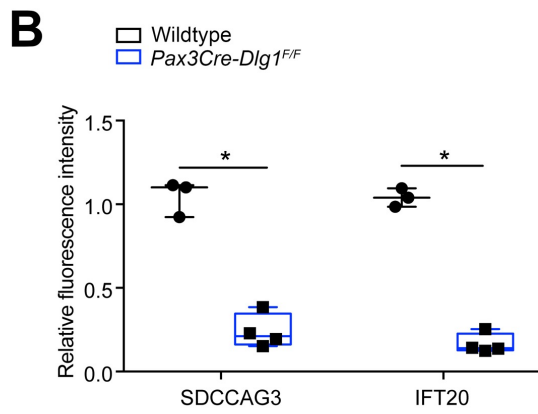
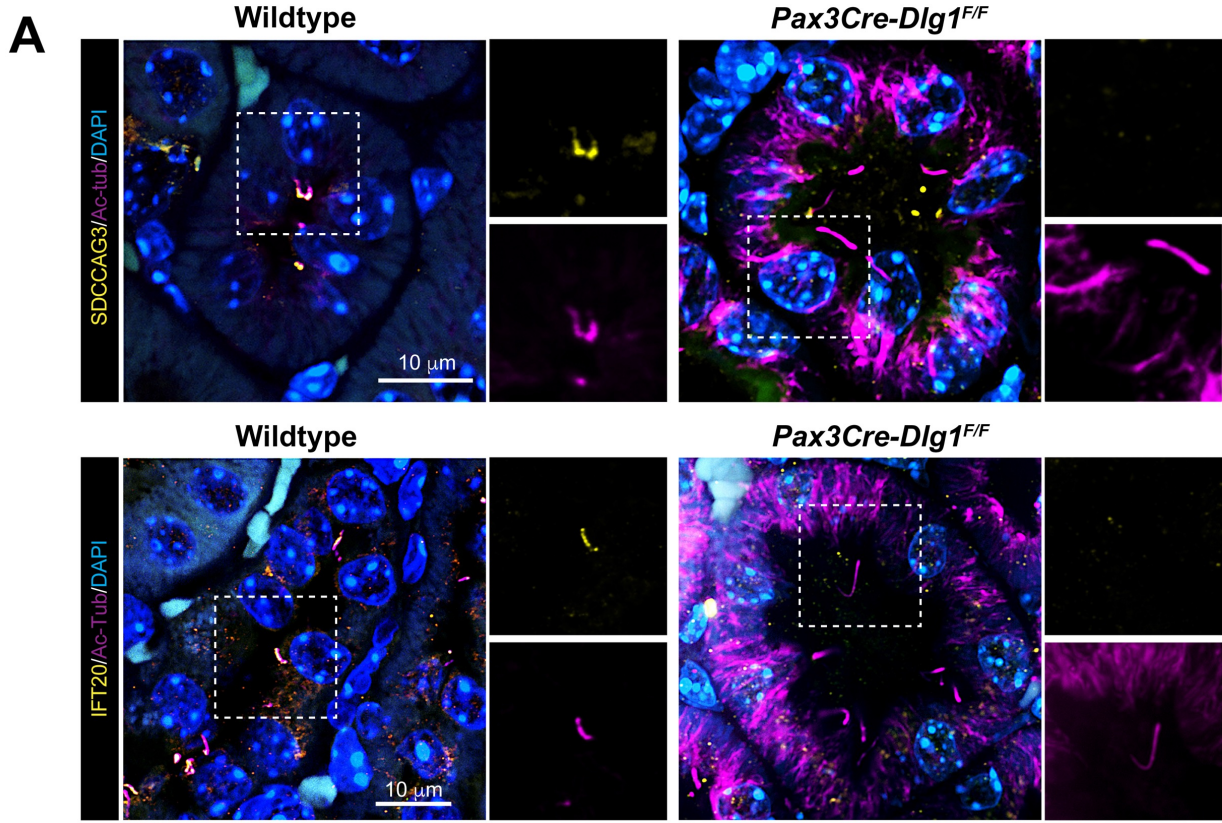
F

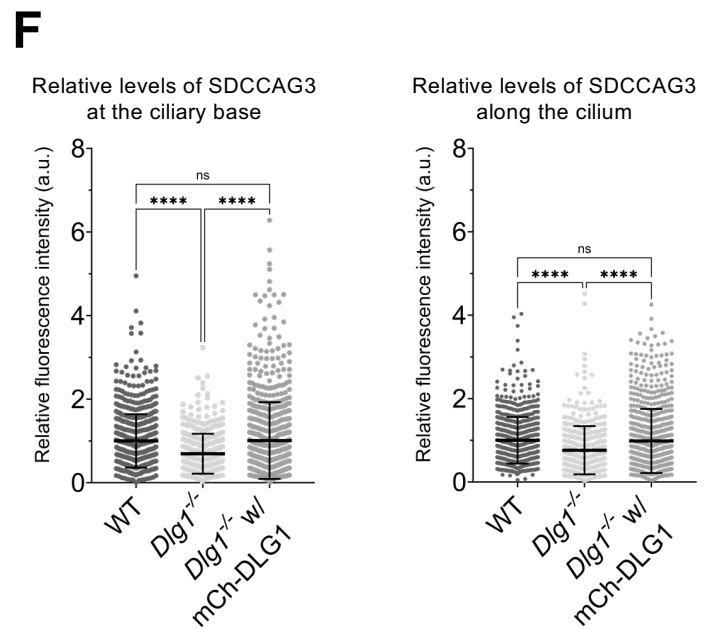
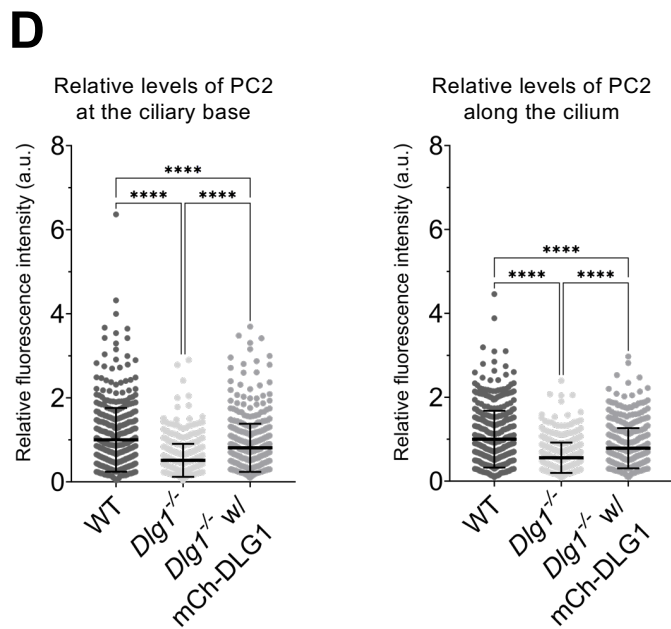
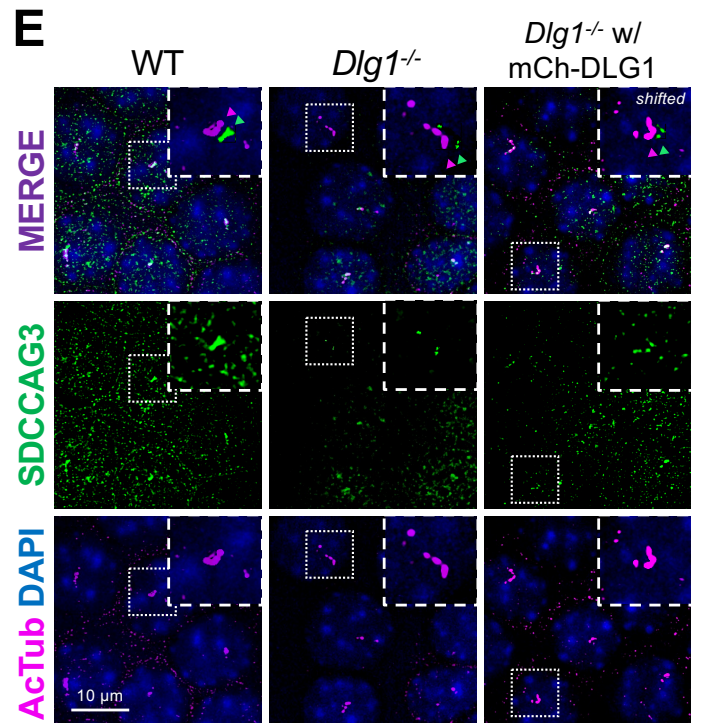
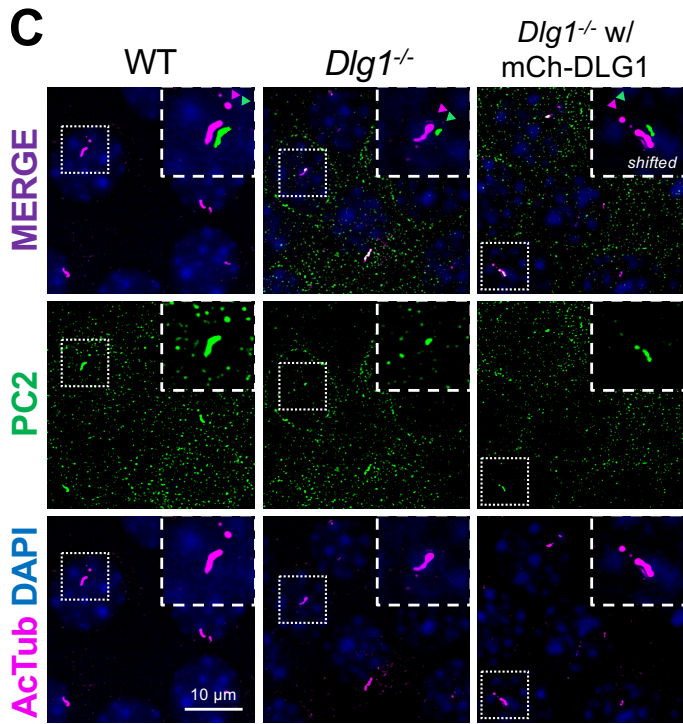
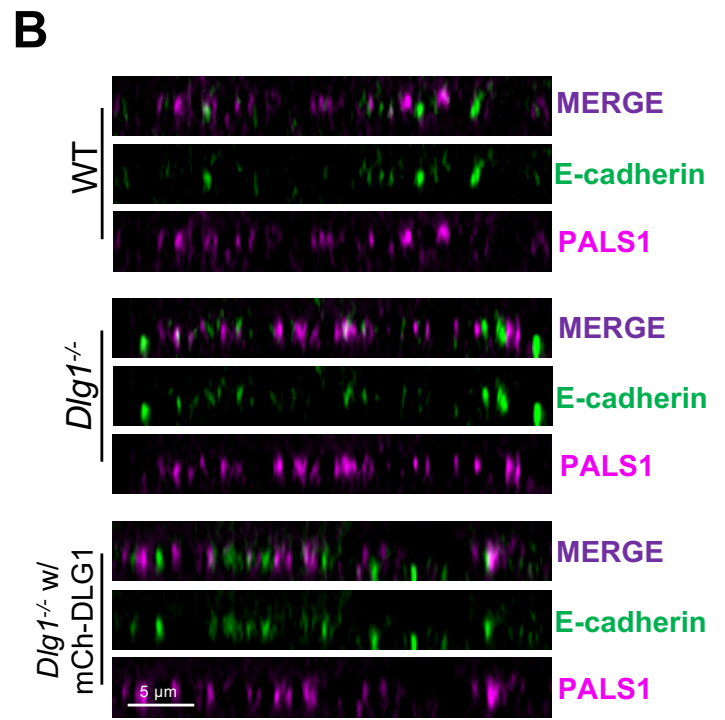
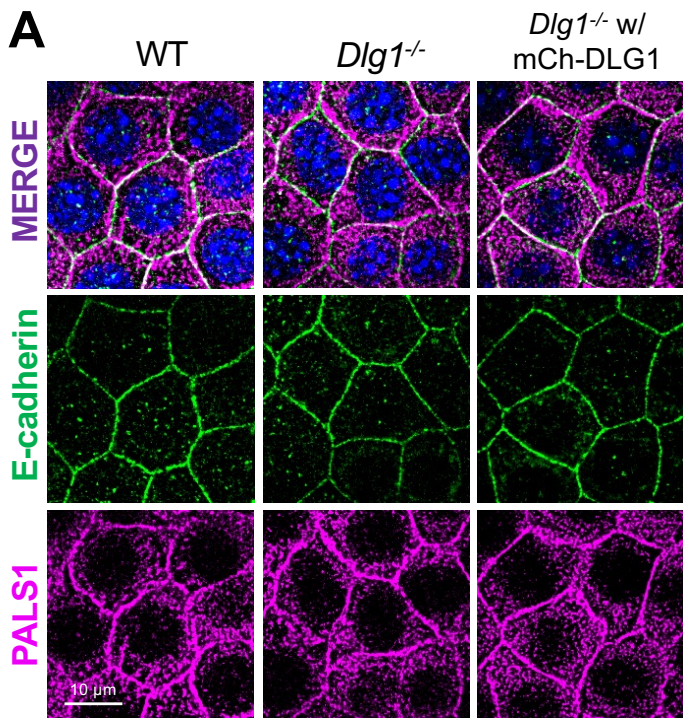
Relative levels of SDCCAG3 at the ciliary base

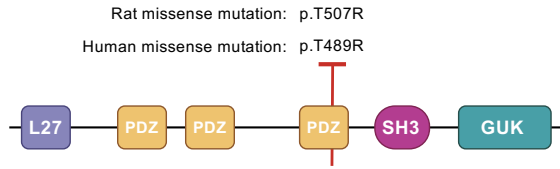
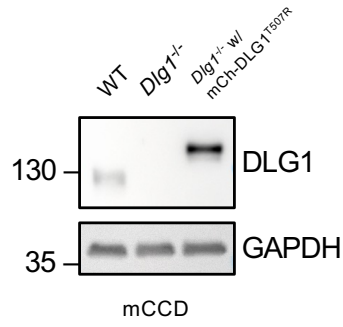


G

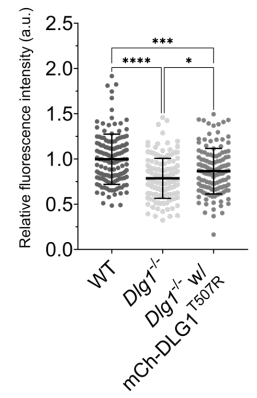
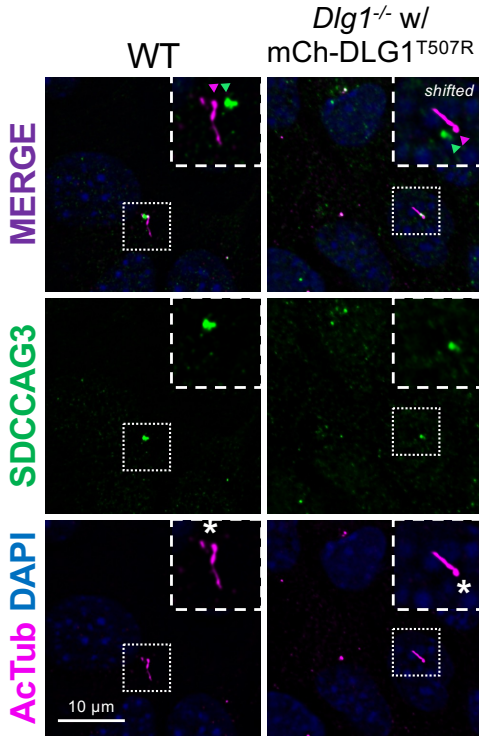
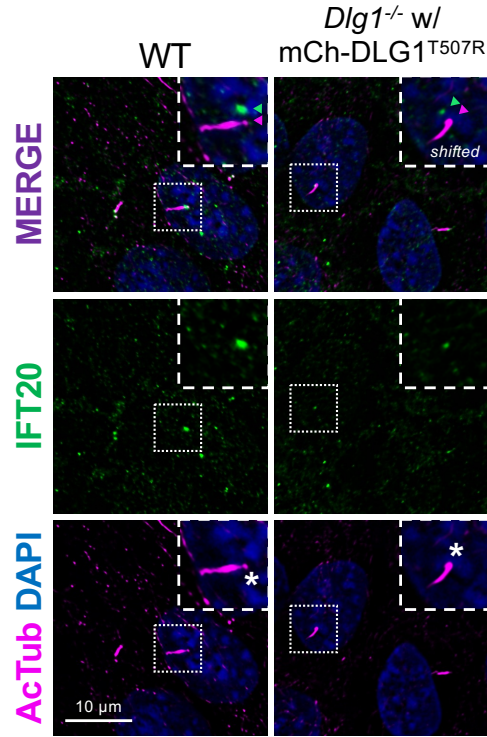




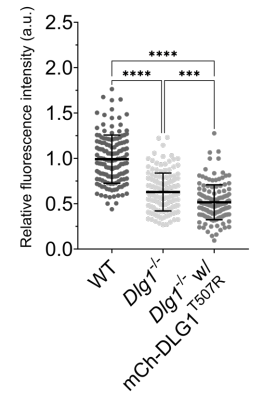
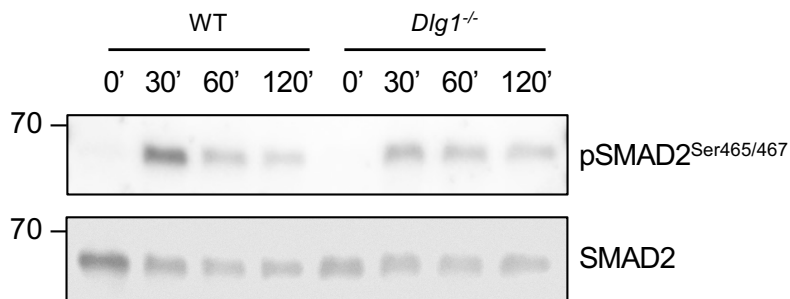
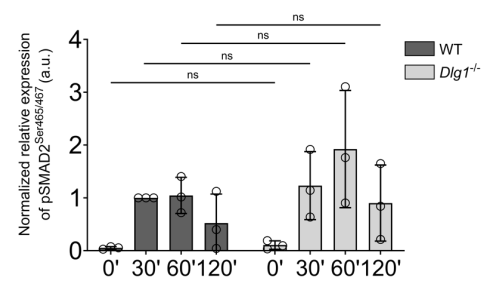
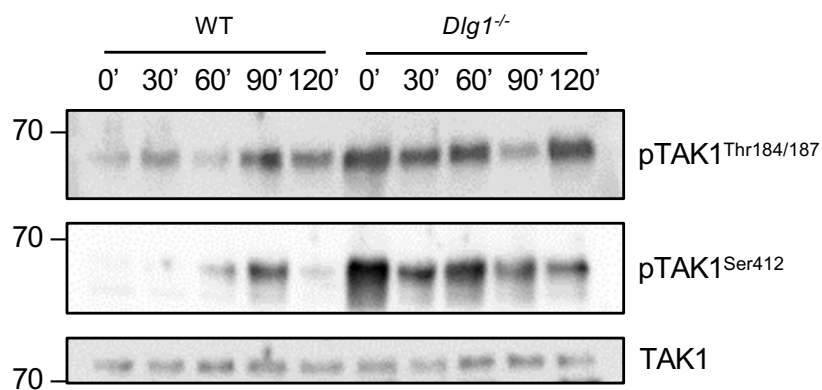


A**B****C**

Relative levels of SDCCAG3
at the ciliary base

**D****E****F**

Relative levels of IFT20
at the ciliary base

**G****H****I****J**